Geological Quarterly, 2024, 68, 43
DOI: http://dx.doi.org/10.7306/gq.1771

Multiple friction tests under low load conditions: application to planar fractures in a shale reservoir

Marek JAROSIŃSKI[1], Radomir PACHYTEL[1, *] and Michał DZIKOWSKI[2]

[1] Polish Geological Institute – National Research Institute, Rakowiecka 4, 00-975 Warszawa, Poland; ORCID: 0000-0003-3084-0644 [M.J.], ORCID: 0000-0001-9407-7233 [R.P.]

[2] University of Warsaw, Faculty of Physics, Pasteura 5, 02-093, Warszawa, Poland; ORCID: 0000-0001-5709-7235

Jarosiński, M., Pachytel, R., Dzikowski, M., 2024. Multiple friction tests under low load conditions: application to planar fractures in a shale reservoir. Geological Quarterly, 68, 43; https://doi.org/10.7306/gq.1771

Associate editor: Piotr Krzywiec

Knowledge of the friction coefficient on fracture surfaces within tight reservoirs, geological storage systems, and the seals of conventional reservoirs, is increasingly important in the geomechanical analysis of fracturing treatment and the assessment of seal integration. We measured the static friction coefficient (μ) of 118 samples of bedding fractures and 52 samples of tectonic fractures taken from a borehole core from the depth interval of 3-4 km in the early Paleozoic Baltic Basin shale reservoir (North Poland). In total, 3372 measurements of μ were made. Based on repeated measurements under the same loading and wetting conditions, the repeatability of the data obtained was evaluated. A significant reduction of the μ value with increasing load was determined, due to the wetting of fracture surfaces. The gradient of μ value decrease caused by the increase in load was compared with predictions for realistic ranges of parameters estimated on the basis of Barton's empirical law. For groups of fractures with similar μ values, the trends are comparable with Barton's predictions and the gradients systematically decrease with decreasing μ. This allowed a rough extrapolation of values measured under very low-load reservoir conditions.

Key words: multiple shear test, static friction coefficient, fractures, shale reservoir.

INTRODUCTION

Shale successions are usually naturally intensely fractured, both along bedding surfaces and as tectonic origin failures (Gale et al., 2014). During the hydraulic stimulation of tight reservoirs, such mechanical discontinuities can be sheared or opened by increased fluid pressure, depending on the present-day stress conditions on their surfaces (Zoback et al., 2003; Aimene and Ouenes, 2015). Due to the action of tectonic forces, most fractures have shear stress at their surfaces that may trigger shear displacement. Estimations of energy release recorded by the monitoring of microseismic events during hydraulic fracturing indicate that such shear fracture stimulation is very common and can be generated even by millimetric displacement on a 1 m^2 surface (Maxwell, 2011; Bachmann et al., 2012). When, due to a high fracking fluid pressure, shear reactivation takes place under decreased effective stresses, the fracture wall asperities are not destroyed and are able to maintain the open cracks. Such naturally propped fractures contribute to an increase in the effective permeabili tyof a reservoir (Gu et al., 2016). Other than by the stress conditions, such shear mode fracture reactivation is controlled by peak shear strength, which is expressed by a static/peak friction coefficient on the fracture surface. A comprehensive geomechanical model of a fractured reservoir, taking into account the spatial relationships between principal stress axes and fracture orientations, can predict whether the reactivation of pre-existing tectonic structures or new hydraulic fractures will develop as a result of increased fluid pressure causing fracturing. In such a model, the static friction coefficient, which controls the level of shear stress required to initiate slip, plays a critical role. If the orientation of the structures is favorable for reactivation, lower pumping pressures can be planned and the proppant selected accordingly, as this plays a lesser role in maintaining reservoir permeability if the fractures are supported by natural asperities. Friction on pre-existing fractures also influences hydraulic fracture propagation and arrest (Anderson, 1981; Eshiet and Sheng, 2017). A low friction coefficient on bedding interfaces favours the mechanical decoupling of layers that eases the arrest of hydraulic fracture propagation (Renshaw and Pollard, 1995; Cooke and Underwood, 2001).This coefficient is also important for wellbore stability considerations (Liu et al., 2010; You et al., 2014; Yan et al., 2018). For example, the friction in the inclined borehole sections of both the tectonic and bedding fractures may be equally important.

* Corresponding author, e-mail: radomir.pachytel@pgi.gov.pl

Received: March 22, 2024; accepted: November 12, 2024; first published online: December 23, 2024

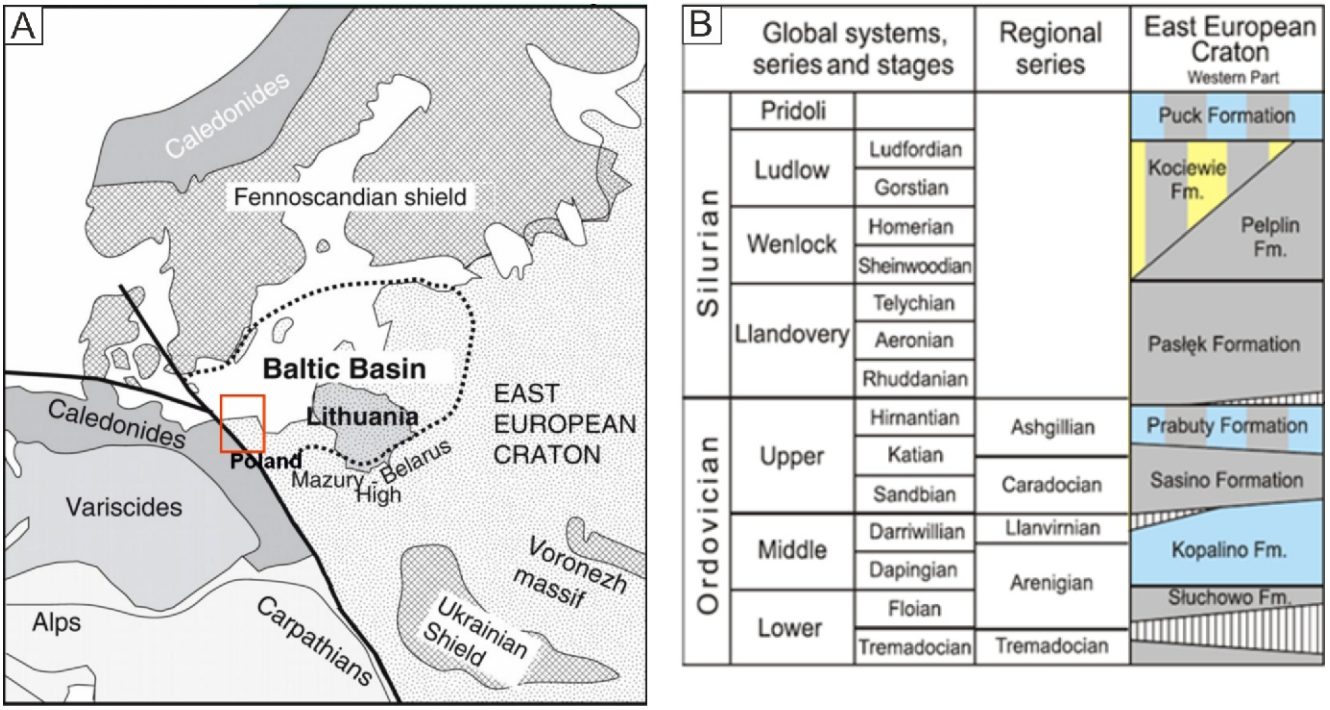

Fig. 1A – borehole data location map (Bobek and Jarosiński, 2021, modified); B – lithostratigraphy of the lower Paleozoic shale succession (Modliński and Podhalańska, 2010, modified)

Grey – claystone and mudstone, yellow – sandstone and siltstone, blue – limestone and marl

The static friction coefficient is the ratio between the maximum tangential and normal stresses to the fracture surface at the moment the shear displacement is triggered. The suggested methods for determining the shear strength are given by the International Society of Rock Mechanics (SM for Determining Shear Strength – 1974 in: Chapter 2 – Laboratory testing, ISRM, 2007), which were revised by Muralha et al. (2014). Except for the rare cases of the friction coefficient being measured in the field on large fracture surfaces, which is not applicable to reservoirs at a depth of several kilometres, the ISRM recommends laboratory friction tests on borehole core samples. Conventionally, direct shear testing is conducted with a constant normal load applied to the discontinuity plane, which is appropriate for the determination of the peak friction coefficient. The maximum shear strength can be estimated also under constant normal stiffness boundary conditions. Such tests, as recommended to study friction at non-planar fractures, always lead to heavy wear of the surface examined. Strongly recommended by the ISRM, but rarely performed, are multi-stage shear tests of fracture strength. For a certain uniform rock volume containing fractures, shear strength can be measured at several fracture samples, under different magnitudes of the constant normal load or stress. This always poses the challenge of collecting a homogeneous set of fractures with comparable friction parameters. In the field, several samples can be taken from one fracture, but this is typically not possible while sampling a borehole core. Alternatively, in a multi-stage test, the same fracture specimen can be sheared repeatedly under different or constant normal load conditions. At least three load steps in increasing load order are necessary to determine friction coefficient changes (ISRM Suggested Method for Laboratory Determination of the Shear Strength of Rock Joints: Revised Version in ISRM, 2015). In such an experiment, a continuous displacement in subsequent load steps can be applied, or repositioning of the sample to its initial position can be repeated after each measurement. The last kind of test is more applicable for the determination of peak shear strength, in which the initial fracture morphology is important. In general, the scarcity of borehole core data, and the destructive character of shear strength tests, mean that the number of such multiple tests from shale reservoirs is very limited.

In the course of structural profiling of borehole core from a shale reservoir in the lower Paleozoic succession of the Baltic Basin (north Poland), we found hundreds of tectonic and bedding fractures (Bobek and Jarosiński, 2021). Taking advantage of this, we decided to systematically measure the static friction coefficient (μ) of the fractures, which parameter being usually undetermined for shale reservoirs. Such supplementary measurements were to be made in core storage, using a fast and non-invasive test method, meaning without the destruction of the core sample and fracture surfaces. With these limitations, we designed a multi-stage shear strength test, under very low load conditions using three load steps in wet and dry conditions. In this paper we provide an analysis of the repeatability of the μ measurements obtained. The trends for μ vary and their significance was tested using statistical analysis. Finally, we discuss the possibility of interpreting our measurements in terms of Barton's law of friction.

GEOLOGICAL CONTEXT OF THE FRACTURE DATA

For our experiments, we had access to continuous borehole core profiles from six vertical boreholes drilled by the Polish Oil and Gas Co. The boreholes were located in the Pomeranian (Polish) part of the Ordovician and Silurian shale succession of the Baltic Basin (Fig. 1A; Poprawa, 2020). The fracture samples

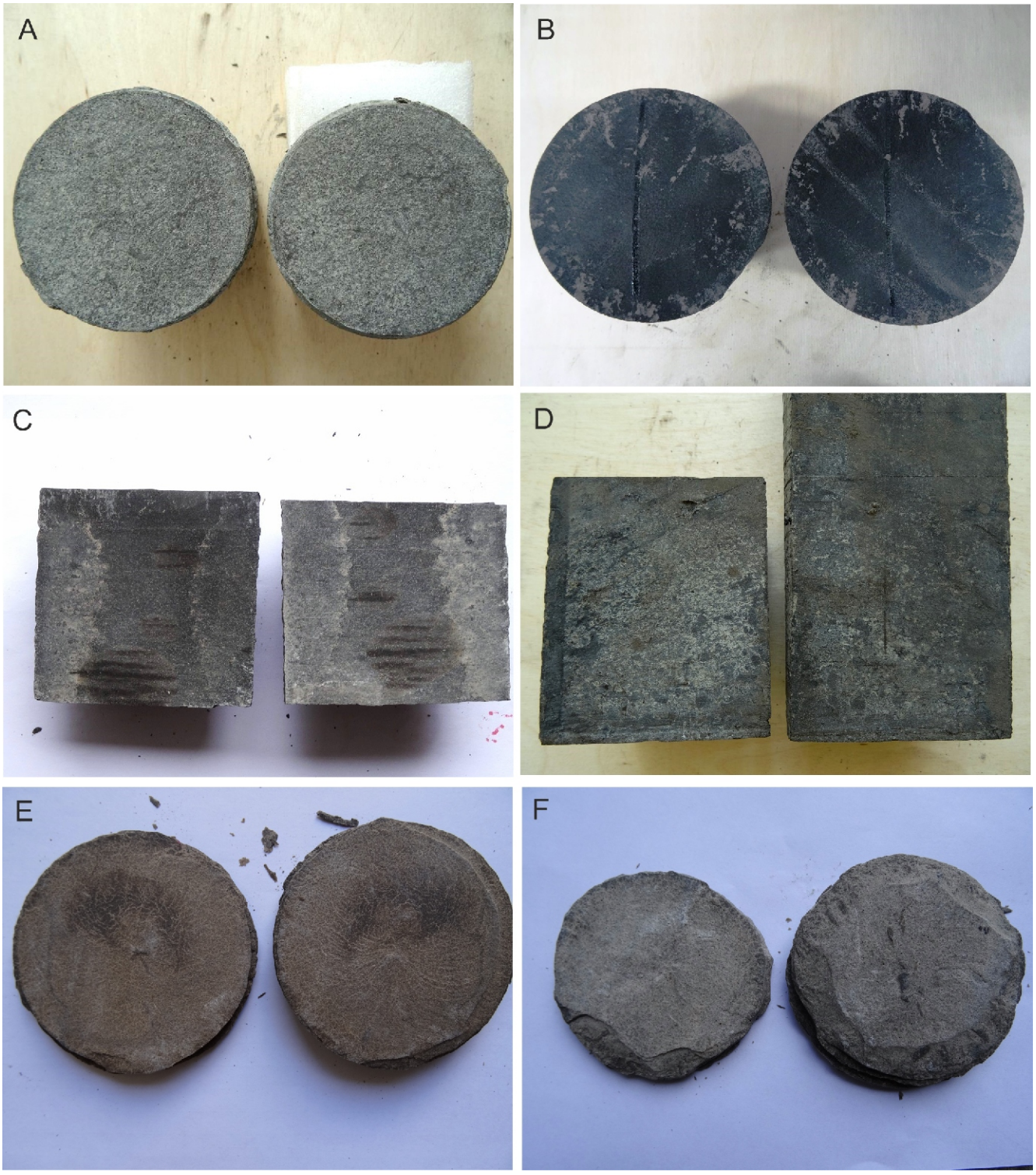

Fig. 2. Examples of the fracture surfaces analysed: A, B – bedding fractures; C, D – tectonic fractures; E, F – tuffite/bentonite bedding planes

analysed are from five shale formations (Fig. 1B; Podhalańska et al., 2020). The most prospective are the Sasino and Jantar black shales, of mean total organic carbon content (TOC) >2%. These formations are separated by the carbonate-rich Prabuty Formation. The uppermost, Pasłęk and Pelplin, formations, have a mean TOC <1.5 %. The Pasłęk, Jantar and Sasino formations contain several tuffite/bentonite intercalations that cover the bedding fractures.

The entire succession analysed is heavily fractured along the horizontal bedding planes (BFr) and as vertical tectonic (TFr) fractures. The BFrs are usually smooth and planar as a result of the flattening of clay mineral laminae due to compaction (Fig. 2A), with rare major surface roughness created by sedimentary features. The TFrs are mostly planar and strata-bound joints (Fig. 2B) of extensional origin (type I) (Ramsay and Huber, 1987) triggered by natural hydraulic frac-

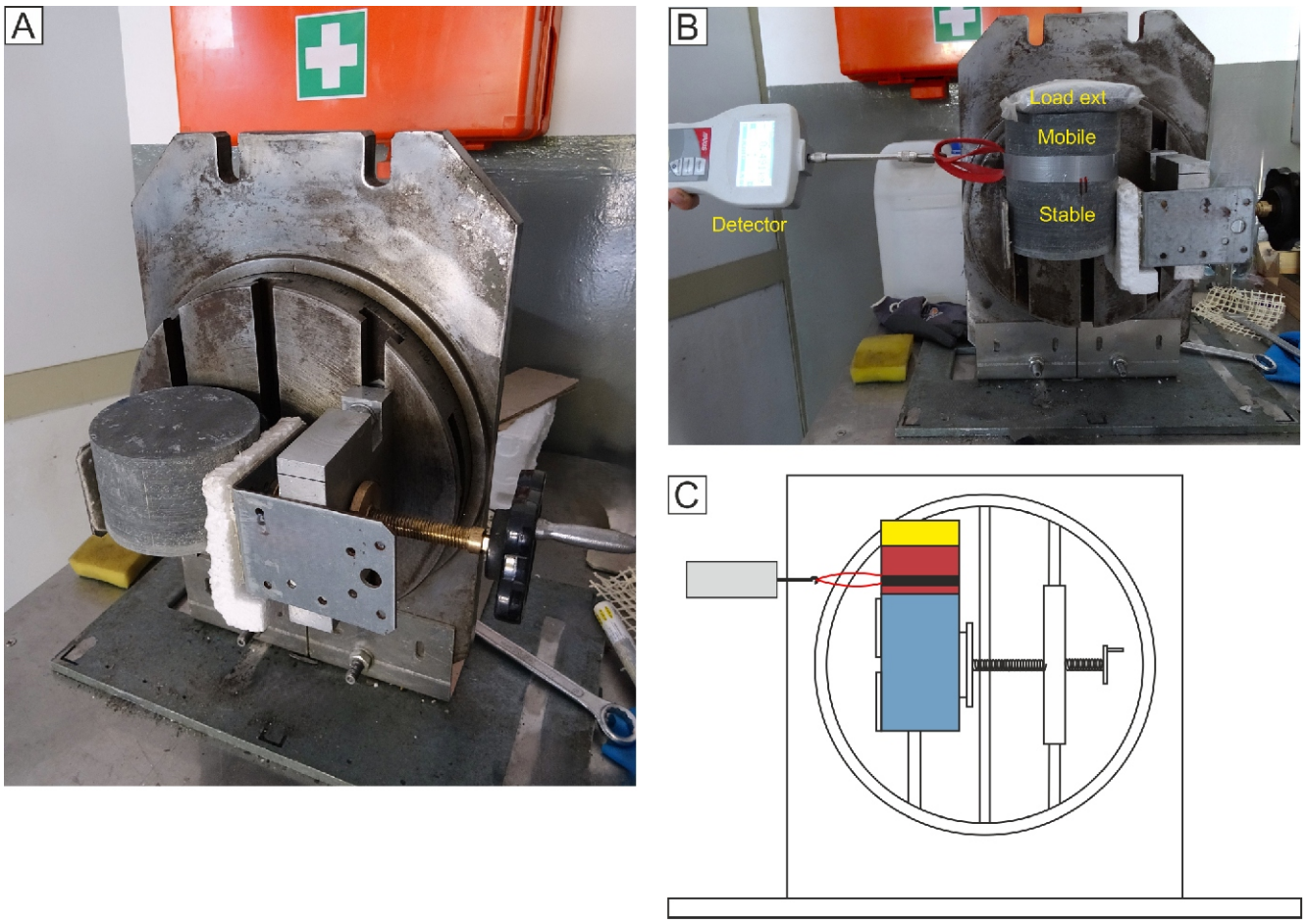

Fig. 3. The apparatus used for static friction coefficient measurements after setting the stable part (A); set, levelled, loaded sample (B) and measurement scheme (C)

Blue indicates the stable part of the sample, red the mobile sample, with yellow for the load extender

turing (Bobek and Jarosiński, 2018, 2021). The surfaces of joints are rarely polished by shear-mode tectonic reactivation, while being frequently filled with calcite, typically creating 0.01–0.5 mm thick veins. The veins are secondarily cracked either tectonically or due to relaxation during borehole core retrieval to the surface (Engelder et al., 2009; Gale et al., 2014). The cracks split veins either along the central suture, a feature of syntaxial veins, or at the mineral infill/host rock interface, common for antitaxial veins (Ramsay and Huber, 1987). In both cases, the mechanical properties of TFr surfaces are not only controlled by the host rock matrix properties, but also by mineralization. Subordinate fractures created by slickensides are not included in this study.

While studying natural fractures in shales, one should differentiate these from drilling-induced fractures (Lorenz and Cooper, 2017), the origin of which is triggered by technological stress and pressure amplification in the near-borehole zone (Kulander et al., 1990). The latter are e.g. core-disking resembling BFr, or centreline fractures similar to joints (Lorenz and Cooper, 2017). However, the specific features of the induced fractures, such as their surface relief or geometry with respect to the core, are diagnostic. If BFrs and TFrs are present, their density typically varies in the range of 2–6 fractures per metre (Bobek and Jarosiński, 2021). In our study, we use the more general term “fracture”, instead of “joint” (used commonly in engineering studies), due to the different origins of these two structures. Following this, we have distinguished three genetic groups of fractures: (1) bedding fractures (BFr); (2) tectonic fractures (TFr); and (3) tuffite/bentonite bedding planes (Tuf). The first two groups were analysed systematically, while the last was only noted occasionally.

THE EXPERIMENTAL SETTING

Our direct shear experiment has been performed using a self-made device (Fig. 3). The lower part of the specimen was fixed in the holder, which allows for a simple levelling of the fracture plane. The force normal to the fracture plane is generated by a gravity load of weights exerted on the upper, mobile part of the sample. This mobile part is pulled horizontally by a dynamometer. During the shear motion of the upper sample, the fracture-normal force is kept constant. The tests at each fracture were conducted in several load steps, which were similar for dry and wet conditions.

MEASUREMENT STEPS

The details of our experiment are given below:

Fracture sample selection. Different fracture types should be represented in the friction tests in proportion to their occurrrence. The samples chosen had to be mechanically

strong, to allow them to be fixed in the apparatus. This condition was not fulfilled by ~50% of the tectonic fractures (TFr) observed and by 20% of the bedding fractures (BFr), among which the thicker tuffite/bentonite beds are especially fragile or prone to disintegration. The fracture surface should lack macroscopic locks or barriers that can prevent displacement under low shear stress. As smooth fracture planes were common in the shale, only a few fractures possessed locks that made measurement-taking impossible.

Measurement of the fracture surface area. Due to the orthogonal position of borehole axes to the bedding (dipping at <3°) areas of the BFr were determined from the simple circular geometry of the core planar intersection (Fig. 3). In the case of more complex TFr geometries, their surface areas were measured from outlines drawn on paper using a planimeter.

Weighing of the mobile part of the sample was performed using a laboratory scale accurate to 0.001 kg.

Holding the immobile part of the sample. The lower part of the sample was fixed in the measuring device with a screw holder, using rubber and polystyrene pads in order to prevent the point indenting or crushing the sample. While being emplaced, the fracture surface was horizontally levelled.

Fixing rubber to the mobile part of the sample. A rubber buffer was used to avoid a rapid increase in tangential load and undesirable dynamic effects while pulling the sample. To avoid the tendency of the sample to rotate in the vertical plane while pulling, the rubber was fixed close to the fracture plane with tape. Rotation in the horizontal plane was minimized by fixing the rubber in the direction of pull. The rubber stiffness was adjusted to the shear force in order to minimize the mobile sample displacement after its first motion, to avoid unnecessary destruction of the fracture surface.

Positioning the fracture walls. Two parts of the sample were carefully placed against each other with the mobile part being on top. The original juxtaposition of fracture relief on both fracture walls was easy to detect manually, and facilitated by means of scribes made on the core.

Normal loading of the fracture surface. A constant load normal to the fracture surface was applied gravitationally by the moving part of the specimen and additional extenders were attached. Lead buckshot was used as extenders with the size of bags similar to the diameter of the samples, which made it easier to find the central position of the load against the sample. The weight of each extender was 1 kg.

Shear loading of the fracture plane. The shear load was applied by pulling the dynamometer which was fixed through the rubber loop to the mobile part of the sample. The rubber was stretched gently in the horizontal direction until the first motion of the mobile part of the specimen was detected. The peak shear force was automatically recorded by the dynamometer with a nominal accuracy of ±0.1% and units accurate to 0.01 N, as described by its manufacturer. In all measurements of the same sample, the shear load was always applied in the same direction.

Sample repositioning. After each measurement, the dust from the fracture surface abrasion was blown away (dry experiment) or wiped with a wet sponge (wet experiment). Then the mobile part of the sample was placed at its initial position and the shear experiment was repeated.

EXPERIMENTAL CONDITIONS

The measurements were done in a closed room, at the borehole core storage facility. Each fracture sample was first sheared under dry conditions, and then the same experiment was repeated under wet conditions. Both dry and wet experiments were performed in three load steps with three repeated measurements for each load step. This resulted in 18 measurements performed for one fracture sample, applied always in the same sequence. During the initial experiments, dedicated to constraining fracture wear, the number of measurements was doubled, giving 36 measurements per fracture.

In the first load step, the weight of the mobile part of the sample was increased by using a 1 kg extender; in the second load step, by 2 kg of additional load; then in the 3rd load step, by an additional 3 kg, totalling 6 kg of extenders plus the weight of the mobile part of the sample. In a few cases, due to sample integrity problems, a maximum of 5 kg extender weight was applied. The maximum load in the experiment was limited by the requirement of a non-destructive test, as well as by the construction of the measuring device. A full test of 18 measurements on one fracture took 10–15 minutes.

The dry experiments were performed on air-dried samples, which had been in storage for 1–3 years. The temperature during measurements was in the range of 16–24°C. For wet experiments, the fracture surfaces were slightly moistened with a wet sponge so as not to flood the sample. We discovered that an excess of water on the fracture surface may cause inadvisable sticking of the fracture walls induced by water surface tension, which influenced the results of our low load tests. The shear test started immediately after the sample wetting. Both wetting and cleaning of the fracture surface were repeated before each repositioning of the sample. By using a small amount of water, which evaporated immediately after the test, we minimized shale-water reactions that might soften the fracture surface.

RESULTS OF THE MULTI-STAGE SHEAR EXPERIMENTS

RAW RESULTS

Altogether, we examined 183 fracture samples, for which a total of 3372 individual measurements were completed. Among these, there are 118 bedding plane fractures (BFr), 52 tectonic fractures (TFr), and 13 tuffite/bentonite bedding planes (Tuf) (see Appendix 1). Due to significant genetic differences between these three groups of fractures, their results are presented separately. Only two tests were not completed due to the disintegration of the samples; for the remaining samples, μ was determined. In each test, the load normal to the fracture plane, F_n was applied and the maximum shear force, F , tangential to the fracture surface, was measured. Dividing these forces by the fracture's surface area results in the determination of normal stress ($_N$), and tangential stress ( ), respectively. From the above stress data, assuming a lack of cohesion on the open fractures, the friction coefficient μ was calculated using the formula (Amontons, 1699):

$$/ \quad _N \qquad [1]$$

For each individual fracture, 18 μ measurements were made. We observed that the μ value systematically decreases with increasing $_N$ in the three successive steps, both in dry and wet experiments (Fig. 4). Also, the results of tests in dry conditions are systematically higher than those for wet conditions, for the same fracture and normal load. This raises the question of whether these systematic μ changes are significant, and if they occur due to wear of the fracture surface in repeated tests. These questions are covered in detail in the following chapters, with subsequent extensive discussion.

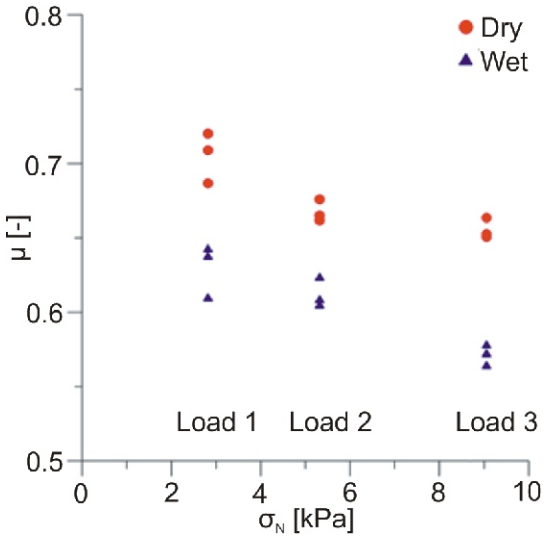

Fig. 4. An example of the test results for one BFr surface, which consists of 18 measurements

Note the more accurate vertical scale with relation to the following diagrams, adjusted to make individual measurements more visible

The collective results of our measurements are shown on the $_N$ and diagrams separately for the TFr and BFr data (Fig. 5). The systematic difference in the results for dry and wet experiments means that both these groups of measurements need to be shown separately. As a result, we obtained four plots where, for clarity, one point represents the average value of the three measurements for each load step. These diagrams illustrate the range of $_N$ applied in our experiments, ranging from approximately 1.5 to 20 kPa. The grouping of points on these charts shows a general upward trend for which the linear regression can be interpreted in terms of Coulomb friction criteria, including cohesion (c) on the fracture surface (Jaeger and Cook, 1979):

$$_N \quad c \qquad [2]$$

In each diagram, the intersection of the linear trend with the axis indicates remnant cohesion in a range between 0.3 and 0.5 kPa. Despite the cohesion being low, its continuous positive value for split fractures may be significant. It suggests that the strength envelope may not follow a linear regression trend even within a narrow range of loads. This could be a consequence of the μ decrease noted with an increase in $_N$. Tentatively, from the inclination of the linear function to the 0X axis the mean values of μ for the fracture sets can be estimated in the range from 0.50 to 0.56. From the simple relation:

$$\arctan(\ ) \qquad [3]$$

the mean friction angle ( ) for the linear Coulomb criteria for the groups examined is estimated to be in the range of 26–29°. Although each group contains a large number of different fractures, the high correlation coefficients R2 obtained (between 0.85 and 0.93) suggest relatively homogeneous frictional properties of the BFr and TFr fracture sets.

WEAR OF FRACTURE SURFACES IN THE REPEATED MULTI-STAGE TESTS

At the beginning of our experiment, we checked whether our measurements influenced the friction properties of the fracture surfaces. After the first friction tests, we observed a small amount of dust remaining on the fracture surface. This dust was blown away from the dry fractures or wiped with a sponge from the wet ones before each successive measurement. Despite this tiny effect, we did not notice any fresh scratches created during tests. To check if this degree of fracture surface abrasion might influence the static friction properties, we organised experiments on three BFr samples with different initially determined μ values. The BFrs were selected due to their higher clay mineral content, that theoretically should make them more susceptible to wear than mineralized TFrs. The values, order, and direction of load application were exactly the same. The difference was that after the first day of the experiment, with 18 measurements in dry and wet conditions performed on each of these three fractures, the samples were dried for 24 hours at ambient conditions, after which another series of 18 measurements were made, repeating the scheme from the previous day. It follows that before each repeated measurement under the same conditions, as many as 18 other friction tests were carried out under various loads and wetting conditions which could influence wear on the fracture surface.

For each sample, the characteristic decrease of μ values was noticed between load steps and between the dry and wet experiments (Fig. 6), similar to those shown previously (Fig. 4). We can also spot that the results for individual load steps from the first day seem to be more dispersed than those from day two. This may suggest a certain smoothing of the fracture surface. To confirm the significance of this effect on the value of μ, we have averaged three μ values for each load step and checked the differences between the first- and second-day results under the same wetting and load conditions (Table 1). We can see that the obtained differences are rather small, ranging from -0.008 to +0.007 which yields less than 1.5% of the average μ value. Although we have obtained a softening of the fracture surfaces in 14 cases, as well as only 4 cases of hardening, the mean range of 18 differences equals 0.002 ±0.004 (~0.5–1% of μ values). For only four cases the softening is slightly higher than the standard deviation of measurements.

Considering the above, we concluded that minor abrasion of the fracture surface does not lead to a significant μ change in our multi-stage shear experiment. Nevertheless, looking at the standard deviation for the sequence of three load steps for each sample, we can observe some predictability. The spread of μ expressed by the standard deviation, in the first load steps is always the highest, while the spread for the third load steps is almost always the lowest. The same applies to the dry and wet tests, in which the standard deviations for dry tests are always higher (mean value 0.009) than those for wet tests (mean value 0.007), considering the same load conditions. These relationships, though minor, were further investigated by analysing hundreds of fracture samples.

WEAR OF FRACTURE SURFACES UNDER LOW LOAD CONDITIONS

The previously described experiment indicated negligible fracture surface wear in the course of multiple measurements under low load conditions. To follow that, we evaluated this rela-

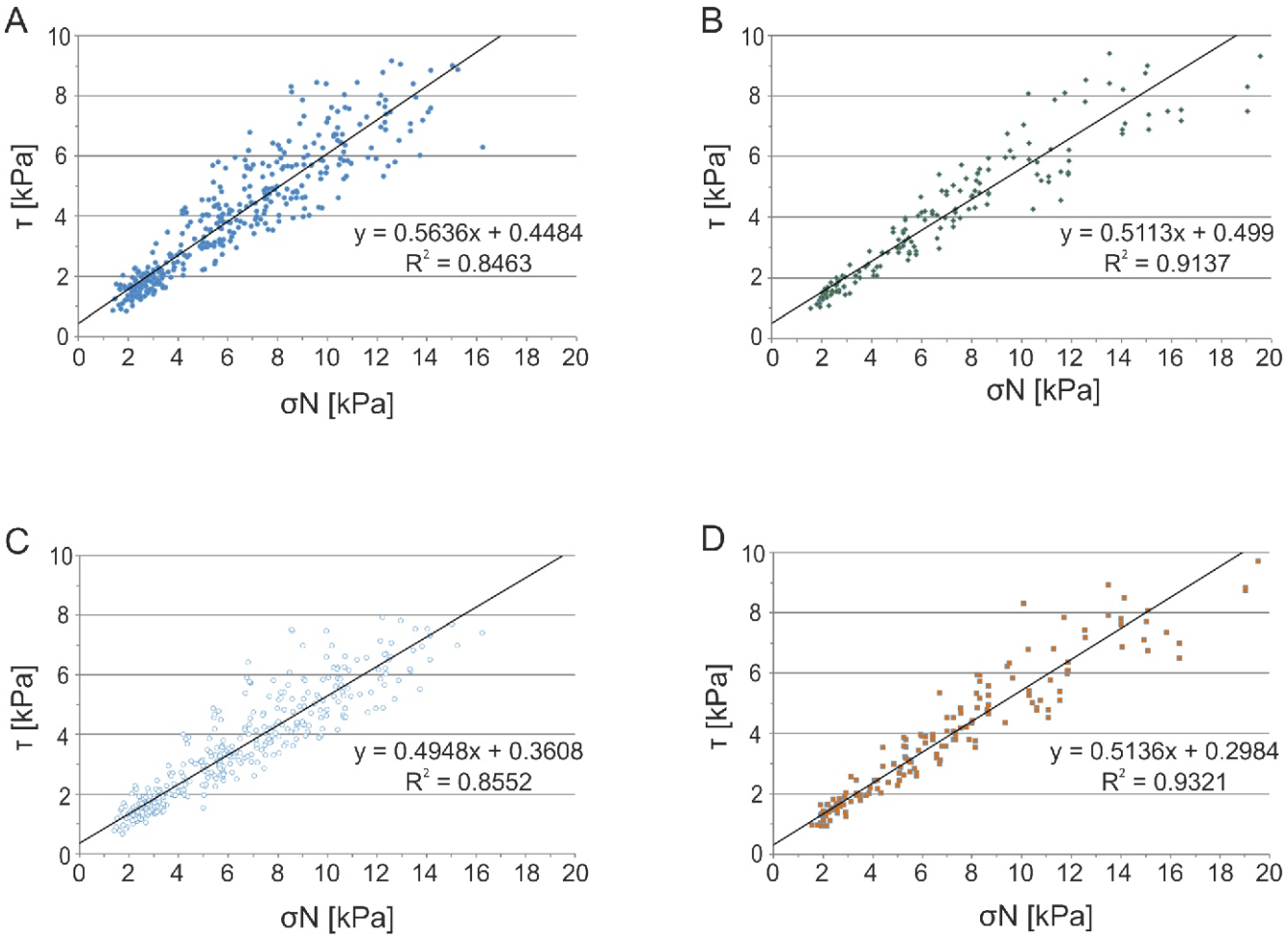

Fig. 5. Stress normal to fracture surfaces vs. shear stress for bedding (BFr) and tectonic (TFr) fractures: A – dry BFr; B – dry TFr; C – wet BFr; D – wet TFr

One point on the diagram is an average of 3 measurements for each load step

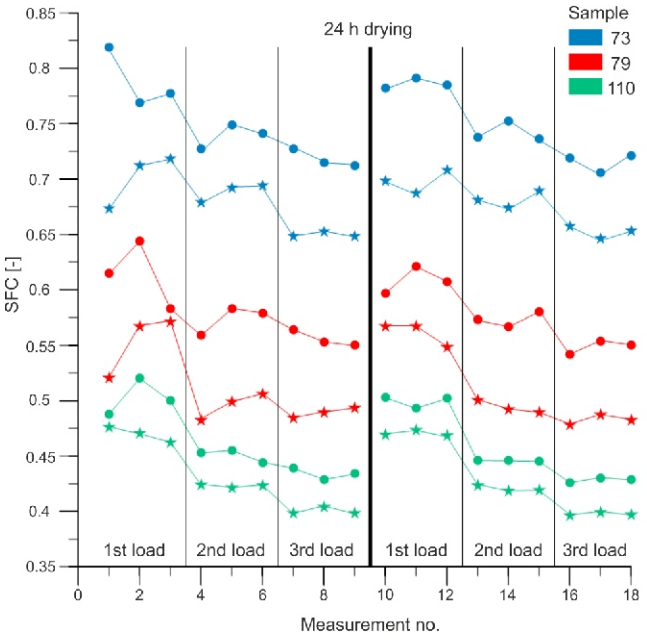

Fig. 6. Two measurement cycles (1–9 and 10–18) testing the effect of surface abrasion in repeated tests. The analyses of dry surfaces are shown as circles while those for wet surfaces are represented by stars

tionship using thousands of measurements. In order to estimate the repeatability/precision of measurements, each sample was measured three times under the same load and wetting conditions. Any change of μ between test repetitions might be attributed to the inaccuracy of the measurement and/or to the wear of a sample. In the first case, the differences between the successive three measurements are random, as long as there is no recurring/time-dependant factor in the experimental setup. From there on, we assume that all errors are random with an unknown mean and standard deviation. In contrast, the wear factor should appear as a systematic rise/drop in friction with respect to consecutive test repetitions under the same load. Since we assume a random character of measurement errors, any systematic changes in friction caused by wear are assumed to be at most linear to the friction length – here understood as equal to the number of test repetitions. Both load and friction length are small, therefore we assume that any significant wear would lead to an approximately linear change in friction during consecutive steps.

Firstly, to justify the use of linear interpolation we evaluated the Pearson correlation coefficient, PCC (Pearson, 1895), between test repetitions for all samples and test conditions. The PCC is an expression of the linear correlation between variables. It ranges from –1 to 1, where 1 is a strictly linear correlation between variables, –1 is a linear correlation with a negative slope, and 0 indicates no linear correlation. Usually, the correlation is assumed strong if the absolute value of PCC is larger than 0.9, but that value limit is a subjective choice. The PCC

Table 1

The results of repeated multi-stage frictional tests on three samples

Sample No.	Conditions	Load step	μ_1 (1st day)	μ_2 (2nd day)	St. dev. for Load Steps	Difference (μ_1–μ_2)
73	dry	1	0.788	0.786	0.016	0.002
		2	0.739	0.742	0.008	–0.003
		3	0.718	0.715	0.007	0.003
	wet	1	0.701	0.698	0.015	0.003
		2	0.688	0.681	0.007	0.007
		3	0.649	0.652	0.004	–0.003
79	dry	1	0.614	0.608	0.019	0.006
		2	0.574	0.573	0.008	0.001
		3	0.556	0.549	0.007	0.007
	wet	1	0.553	0.561	0.018	–0.008
		2	0.496	0.494	0.008	0.002
		3	0.489	0.482	0.005	0.007
110	dry	1	0.503	0.499	0.01	0.004
		2	0.451	0.446	0.004	0.005
		3	0.434	0.428	0.004	0.006
	wet	1	0.469	0.470	0.004	–0.001
		2	0.423	0.420	0.002	0.003
		3	0.4	0.397	0.003	0.003
Mean μ difference ± St. Dev.					0.002 ±0.004	

The μ_1 and μ_2 values stand for the mean from 3 measurements for each load step. The standard deviation is calculated for each load step from the results of 3 measurements

evaluation of all test samples (Table 2) revealed that in the case of tests run under the same load and wetting conditions, the minimum correlation value between repetitions is equal to 0.96 for load step 1, and above 0.97 for the remaining ones, indicating very strong linear correlations between test repetitions under the same load. In other words, it is justified to assume that there is at most a linear change of μ for test repetitions present in the data. It should be strongly emphasized, that while at this point, we assume linear correlation, we will proceed to show that in fact, μ is constant (trivial linear function y = *const.*) with the same load repetitions; we do not observe the influence of wear.

To further investigate the amount of possible wear of a sample, we fitted second-order polynomials to the (normalized by load step averaged) repeated test values. Normalization through averaging gave us the possibility to seek any relation between test repetitions and μ among all the samples, not only per piece. We found that both the cubic and linear interpolation coefficients were below 0.5% of the average μ, with a standard deviation of <3%. Based on that, we concluded that no significant wear was observed during the experiment. Additionally, the relative deviation in a single measure of μ from the average out of all the repetitions under a given load value has a standard deviation in the range of 1.2–3.2% (Table 3) with a mean value of 2.2%, which gives a good estimate of the measurements' precision. In other words, repeated measurements of the same value for the same sample, under the same conditions and the same load, deviate from the average value at those conditions by ±~3% of the averaged value (68% of all cases) and by ±6%

Table 2

Pearson's correlation coefficient evaluation for all fractures in dry and wet conditions, measured between repeated measurements under the same load

	Repetition 1	Repetition 2	Repetition 3
Load step 1			
Repetition 1	X	0.963 (wet)	0.972 (wet)
Repetition 2	0.963 (dry)	X	0.981 (wet)
Repetition 3	0.976 (dry)	0.982 (dry)	X
Load step 2			
Repetition 1	X	0.984 (wet)	0.985 (wet)
Repetition 2	0.991 (dry)	X	0.984 (wet)
Repetition 3	0.987 (dry)	0.988 (dry)	X
Load step 3			
Repetition 1	X	0.986 (wet)	0.993 (wet)
Repetition 2	0.995 (dry)	X	0.986 (wet)
Repetition 3	0.975 (dry)	0.976 (dry)	X

One over diagonal indicates that μ at LS1 in repetition 1 is always equal to itself (Y = 1*X + 0, as Y = X). Values close to 1.0 presented off-diagonal indicate that the relation between μ between repetitions is close to linear (including being identical). In this test, we could use all data sets, as we correlated μ of a given sample under the same load

Table 3

Relative standard deviation of μ in a load step between repetitions

Fracture type	Standard deviation of μ in a load steps					
	LS 1	LS 2	LS 3	LS 1 (wet)	LS 2 (wet)	LS 3 (wet)
BFr	2.4%	1.9%	2.8%	2.4%	1.9%	1.9%
TFr	2.8%	1.7%	1.2%	3.2%	2.1%	1.2%

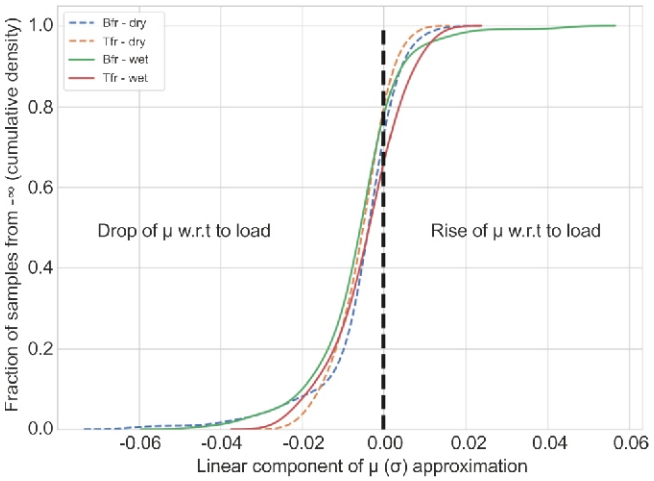

Fig. 7. Linear component of relative friction vs. relative load approximation

It can be seen that almost 80% of the samples show a reduction of friction with increasing load

of the averaged value (95% of all cases). There was also only a minimal difference between sample types, namely the mean standard deviation for BFrs is 2.2% and for TFrs is 2.0%.

To summarize, this data indicates that while a wide range of μ values was measured, this is more likely attributed to individual properties of the fracture samples, rather than the inaccuracy of the experimental setup or the wear of the samples. N.b., the analysis presented attempts to deal with repeatability/precision, which should not be understood as absolute accuracy.

FRICTION COEFFICIENT CHANGES WITH LOAD STEPS

While taking measurements, we observed (e.g., Figs. 4 and 6) that μ systematically decreases with increased load in each following step, and between dry and wet experiments. In our analysis of μ changes for the shale formations, we found a predominance of such trends in most of the cases analysed (Fig. 7).

To analyse this trend, the distribution of μ values for individual load steps was calculated separately for wet and dry samples. In the remainder of this paper, we systematically use the average over the repetitions as the μ value for a given load step. The distribution of μ values in subsequent load steps is presented for complete sets of BFrs and TFrs (Fig. 8).

The μ distribution for BFrs shown resembles a Gaussian distribution, with the exception of the uppermost μ values, above ~0.8 for wet, and 0.9 for dry, samples, which show significant discrepancy from the normal trend. This suggests that the asymmetrical nature of the plot might be attributed to the interlocking of larger-scale features on the fracture surfaces. For dry samples, moderate initial μ values are between 0.633–0.670 (Table 4). In subsequent load steps (LS) μ values indicate a regular decrease by 0.016 and 0.021 which gives 2.4% for LS_1–LS_2 and 3.1% for LS_2–LS_3. Wet samples appear to have both lower μ values and a smaller distribution of them, which is expressed by average μ values between 0.546–0.595. Also evident is systematic μ weakening in successive load steps by 0.031 and 0.018, which gives 5.2% for LS_1–LS_2 and 3.2% for LS_2–LS_3. The μ value drop between dry and wet BFr samples for the same load steps reaches 0.075–0.9, giving a range of μ decreasing by 11.2–13.8%.

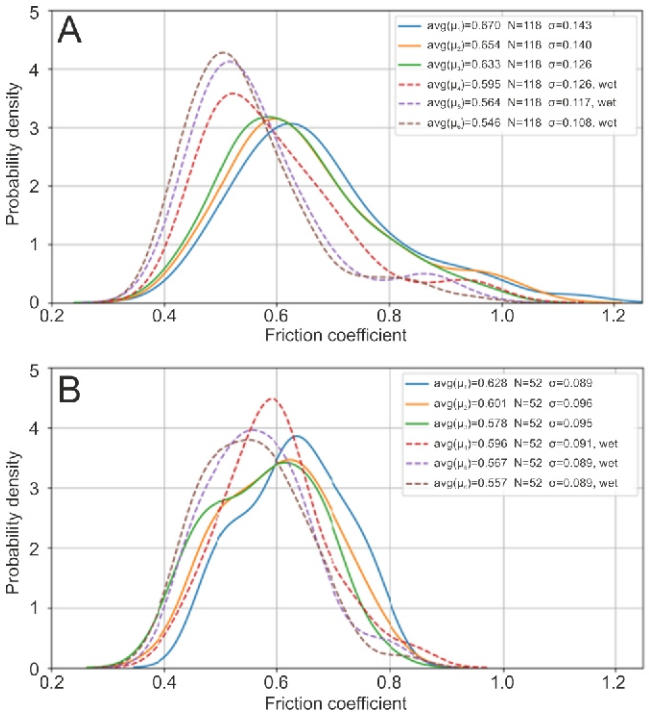

Fig. 8. Distribution of friction coefficient μ separated for three load steps and for dry and wet conditions for BFr (A) and TFr (B)

The plot is normalized in such a way that the integral under it is always equal to 1. Legend shows the average (over samples), the number of samples included, and dry/wet indication

Fewer tectonic fractures reveal a less regular Gaussian distribution of μ values for dry samples, suggesting that there is more than one mode of TFr surface. However, the μ distribution for wet samples is more regular. The mean μ values for dry samples (0.578–0.628) and for wet samples (0.557–0.596) are similar to values obtained for BFrs, although the spread of mean values for load steps is smaller than that for TFrs. The same decreasing trend of μ values for subsequent load steps is visible for dry (by 0.027–0.023) and wet samples (by 0.029–0.010) which gives 2.3–2.7% for dry and 1.0–2.9% for wet samples. The μ value decrease from dry to wet conditions is more evident, falling between 3.6–5.6%. Most of these values are above or comparable to the precision of the measurements, with a mean value of 2.2%.

Such crude analysis does not include the fact that, due to the weight variation of the mobile part of the sample and fracture area, the actual load differs between samples, and this might be part of the reason for the shape of the distribution. To account for that, we evaluated the relative change of μ with respect to the relative change of load, both in terms of normal stress and μ in the first step. This means that point (1, 1) on the plot (Figs. 9 and 10) equals μ and the applied load at the first load step, the same being true for all remaining samples. A decrease on a plot also means a decrease in μ with increasing load. This could be restated as an answer to the question: how many times does μ change (reduces) with an applied load raised by a factor of X. A regression plot for those data, along with distribution indicators, is shown in Figure 9. Red dots are used to indicate the aggregation points and the standard deviation of data points used to create them. Despite the data being highly scattered, the linear fit reveals a decrease of μ value with an increase in load.

Table 4

Range of the mean friction coefficient μ and friction angles obtained for BFrs and TFrs under dry and wet conditions, according to results shown in Figure 8

	Load Step	μ - 2	Mean μ	μ + 2	- 2	Mean	+ 2	SD
Bedding Fractures								
Dry	1LS	0.384	0.670	0.956	21.0	33.8	43.7	0.143
Dry	2LS	0.374	0.654	0.934	20.5	33.2	43.0	0.140
Dry	3LS	0.381	0.633	0.885	20.9	32.3	41.5	0.126
Wet	1LS	0.343	0.595	0.847	18.9	30.8	40.3	0.126
Wet	2LS	0.330	0.564	0.798	18.3	29.4	38.6	0.117
Wet	3LS	0.330	0.546	0.762	18.3	28.6	37.3	0.108
Tectonic Fractures								
Dry	1LS	0.45	0.628	0.806	23.1	32.2	41.3	0.089
Dry	2LS	0.409	0.601	0.793	21.1	31.0	40.9	0.096
Dry	3LS	0.388	0.578	0.768	20.0	29.8	39.6	0.095
Wet	1LS	0.414	0.596	0.778	21.4	30.8	40.2	0.091
Wet	2LS	0.389	0.567	0.745	20.2	29.4	38.6	0.089
Wet	3LS	0.379	0.557	0.735	19.8	29.1	38.4	0.089

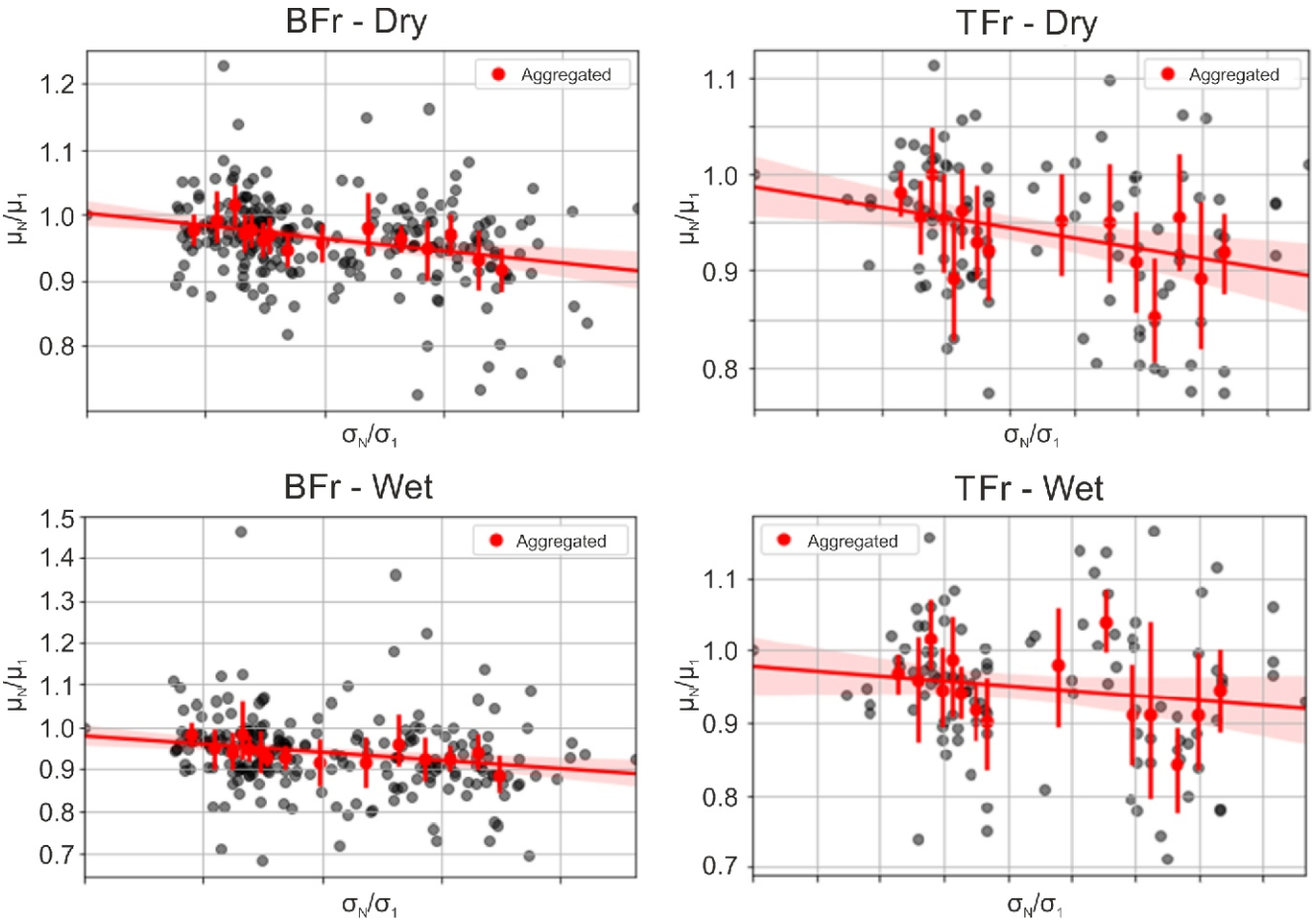

Fig. 9. How many times does the friction coefficient change with an applied normal load change by a factor of Xμ Relative changes in friction as a function of the relative changes of load for bedding fractures (left) and tectonic fractures (right)

The red line is a linear regression, and red dots are aggregated data points with error bars indicating the “density” and “distribution” of data points in a grouping. Data points are first grouped along X, then the standard deviation in Y is calculated (red error bars), along with the average value (red dot)

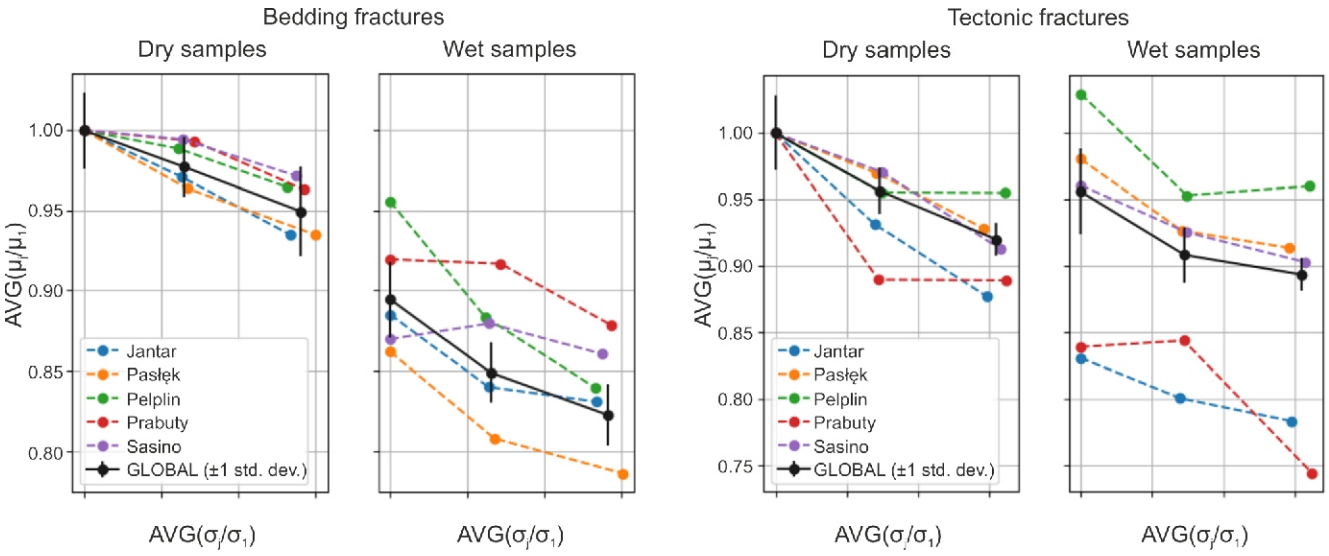

Fig. 10. Cross-plots of the friction coefficient and normal load changes in successive load steps, both calibrated to the mean values for the first load step

Separate diagrams are shown for BFr ("Bedding fractures", two diagrams) and TFr ("Tectonic fractures", two diagrams) for wet and dry experiments. In each diagram, the curves represent results for individual shale formation. Black lines indicate the average μ trend for all formations

The samples are marked also by lithologically defined formations that allowed us to group the samples into more homogeneous subsets of BFrs and TFrs. For such subsets, we checked μ dependence on load and wetting (Fig. 10). Following the previous approach, we examined differences between averaged relative decreases of μ vs. relative load increase (with respect to the first load step). Among the 20 plots, none break away from the general rule of μ decline from LS_1 to LS_3 load steps. Considering the trend cases between consecutive load steps (LS_1–LS_2 and LS_2–LS_3), of which there are 40 cases, there is only 1 case, wet BFr from the Sasino Formation, where friction hardening is evident, while in another 4 cases there is no significant change in μ. Considering the impact of fracture surface wetting on the μ value, 30 dry/wet pairs could be distinguished, out of which only 2 cases violate the rule of μ decrease with wetting, both cases being TFrs from the Pelplin Formation.

Comparing the average trends for all formations (black lines in Fig. 10), weighted by the number of tests in each of them, we can evaluate the μ decrease in each subsequent load step, as well as between dry and wet tests. The overall (LS_1–LS_3) average μ decrease due to an approximate fourfold increase of $_n$ is 5% for dry and 7.5% for wet BFrs, and 8% for dry and 6% for wet TFrs. These decreases are greater than the previously estimated precision of our measurements, on average 2.2% for BFrs and 2% for TFrs. When we look at the average μ decrease in subsequent load steps, we see that in the case of dry fractures the trend is almost linear, but in the case of wet fractures, BFrs and TFrs reveal a greater decrease between LS_1–LS_2 than between LS_2–LS_3. However, this subtle pattern is considered to be at the limit of measurement error. The differences in the decrease of μ between formations exceed 10% for wet BFrs and 20% for wet TFrs.

DISCUSSION: MEANING OF THE FRICTION COEFFICIENTS DETERMINED IN MULTIPLE TESTS UNDER VERY LOW LOADS

MEASURED VARIATIONS OF FRICTION COEFFICIENT AND PREDICTIONS OF BARTON'S LAW OF FRICTION

Comparing the results from repeated measurements under the same conditions, we showed that changes in shear strength between load steps are not caused by wear of the fracture surfaces. The asperity abrasion, observed during the tests, had a negligible impact on the μ value. Similarly to our experiment, a decrease in μ with an increase in normal stress is predicted by Barton's empirical equation (Barton, 1973), which was proposed half a century ago, and still seems to be relevant (Barton, 2013). Its general formula for the shear stress ( ) is:

$$_N \tan \; _b \; JRC \log_{10} \frac{JCS}{_N} \qquad [4]$$

where: *JRC* – the joint roughness coefficient, *JCS* – the joint compressive strength, $_b$ – the joint basic friction angle.

Following the interpretation by Bandis et al. (1981), these parameters represent 3 components of friction at a fracture surface: the geometrical component is expressed by *JRC*, the frictional component is represented by $_b$, and the component for strength (of asperity) is given by *JCS*. Since the term "joint" refers to our bedding and tectonic fractures (BFrs and TFrs), these coefficients may also characterize the factors that control μ in the experiments described. However, there are two major

problems: that the above formula was developed using higher loads than applied in our experiment, and that the coefficients of Eq. 4 were not determined by us. Nevertheless, we are able to evaluate the theoretical μ decrease in the load range used in our experiment (1.5 to 20 kPa), predicted by Eq. 4 when the realistic values of these coefficients are estimated and assumed.

Considering the strength component, *JCS*, it is sometimes accepted that an unconfined rock compressive strength can be assumed (Barton, 1976). The uniaxial compressive strength measurements for one of the boreholes analysed were generally in the range from 20 to 50 MPa (Wojtowicz et al., 2021). We attributed the lower value to BFrs in which the surfaces are weakened by enrichment in clay minerals, and the higher value to TFrs in which surfaces are, at least partially, covered by calcite. Realistic values for the geometrical components, *JRC*, were estimated by visual comparison to the reference fracture profiles (Barton, 1976). It was concluded that JRC values ranging from 1 to 3 should cover most of the fractures. The frictional component, $_b$, is usually determined at smooth surfaces (e.g. saw-cut) under loads of several kPa (Cawsey and Farrar, 1976; Hu and Cruden, 1988), which is comparable to that applied in our experiment. Because most of the fractures analysed have smooth surfaces, we expect that $_b$ is not significantly smaller than the friction angle calculated from the μ value, given in Table 4. Therefore, we assumed that the minimum $_b$ is slightly below the value for mean angles obtained in the 3rd load steps decreased by –2 . With a certain approximation, the lower and upper $_b$ values for wet samples were set at 15 and 30°, respectively. Published values for shale are also reported in this range (Barton and Choubey, 1977).

MECHANISM OF FRACTURE WEAKENING BY WETTING

In our measurements, we observed a systematic weakening of fracture surfaces caused by wetting (Table 4). This well-known phenomenon may result from the weakening of the rock due to clay mineral-water reactions (Jumikis, 1966; Gutierrez et al., 2000), as well as from lubricating the fracture surface with water. Due to the good repeatability of measurement results after sample drying (shown in Fig. 6 and Table 1), we do not expect a weakening of asperities that would result in detectable changes to the fracture surface geometry. Therefore, we can expect that the lubrication mechanism works effectively, causing, as per Barton's law, a decrease in the $_b$ value. The data given in Table 5 indicate that the mean decreases by 3.5° for BFrs and 1.2° for TFrs resulting in the decrease in $_b$.

Table 5

The difference between values in dry and wet conditions for the same loads based on data from Table 4

Fractures	Mean			decrease %
Load step	dry	wet	dry-wet	
BFr 1LS	33.8	30.8	3.0	8,9
BFr 2LS	33.2	29.4	3.8	11,4
BFr 3LS	32.3	28.6	3.7	11,5
Mean drop			3.5	10.6
TFr 1LS	32.2	30.8	1.4	4,3
TFr 2LS	31.0	29.4	1.6	5,2
TFr 3LS	29.8	29.1	0.7	2,3
Mean drop			1.2	4.0

BARTON'S PREDICTION VS. DETERMINED FRICTION COEFFICIENT CHANGES

Even under very low loads we obtained a systematic decrease in μ, the trend predicted by Barton's function. However, this function predicts a non-linear decrease in μ, which is not possible to show in our experiment due to the deviations from the linear trend being at the limit of measurement accuracy. Having not measured any parameters used by Barton's function, we simply compared the mean decreases of μ values in successive load steps (LS) with the values returned by Barton's function in the range of previously estimated realistic parameter values. To do so, we plotted the graphs of μ values as a function of normal stress normalized to the strength coefficient ($_n$/*JCS*) for BFrs and TFrs (Fig. 11):

$$_{Barton} \quad \tan \; _b \; JRC \log_{10} \frac{_n}{JCS} \qquad [5]$$

These figures include only the wet test condition measurements, which are closer to the natural conditions of a reservoir. These graphs, with the 0X axis shown on a logarithmic scale, show that almost all BFr measurements and all TFr measurements fall within the range defined by the Barton function for the estimated range of parameter values. In such a projection, there are only two parameters that determine the course of this function: $_b$ causes a translation of the graph in the 0Y direction, and *JRC* controls the gradient of the μ decrease. The trend lines of the average measured μ values' decrease (thick black lines in Fig. 11), despite their large variation, reveal a pattern. For large initial μ values, defined by μ >0.7 for the first load steps, for both BFrs and TFrs, we obtained the steepest gradients of μ decrease, which exceed the gradient predicted by Barton's equation for *JRC* = 3. It follows that among fractures with high friction there are probably some, where displacement is blocked by larger-scale elements giving a higher effective *JRC*. The same conclusion was made, based on deviations from the Gaussian distribution of μ values, for BFrs. For the group of fractures with moderate μ values in the first load step (0.5–0.7) the gradient of μ is negative and less steep. Its trend is within the range predicted by Barton's function for the mean parameter values, approximately *JRC* ~2 and $_b$ ~22°. While for the weakest fractures with μ values in the first load step <0.5, the declining trend lines for BFrs and TFrs are gently inclined, similar (BFr) or even lower (TFr) than the prediction of Barton's function for the minimum values of the JRC ~1. Such results consistently show that an increase in the initial μ value is accompanied by an increase in *JRC*. From this plot, the mean effective *JRC* value can be estimated in the range from 0.5 to 4. From the graph analysed (Fig. 11A) it is also clear that the lower μ values are attributed to BFrs infilled with tuffite/bentonite (red dots). For some of these fractures $_b$ <15° or/and *JRC* <1 can be attributed.

EXTRAPOLATION OF FRICTION COEFFICIENT TO STIMULATED RESERVOIR CONDITIONS

The question still remains: whether we can use measured μ values in reservoir analysis? Considering that the shale successions studied are at a depth of 3 km or more, the minimum natural lithostatic pressure exerted on them is ~75 MPa. However, during hydraulic fracturing, high fracking fluid pressure is used that locally, in the near-borehole zone, is able to overcome the lithostatic pressure. Therefore, shear activation of natural fractures in the stimulated part of the reservoir can be triggered even under very low effective normal stress. Then, the effective normal stress during shear of a pre-existing fracture is depend-

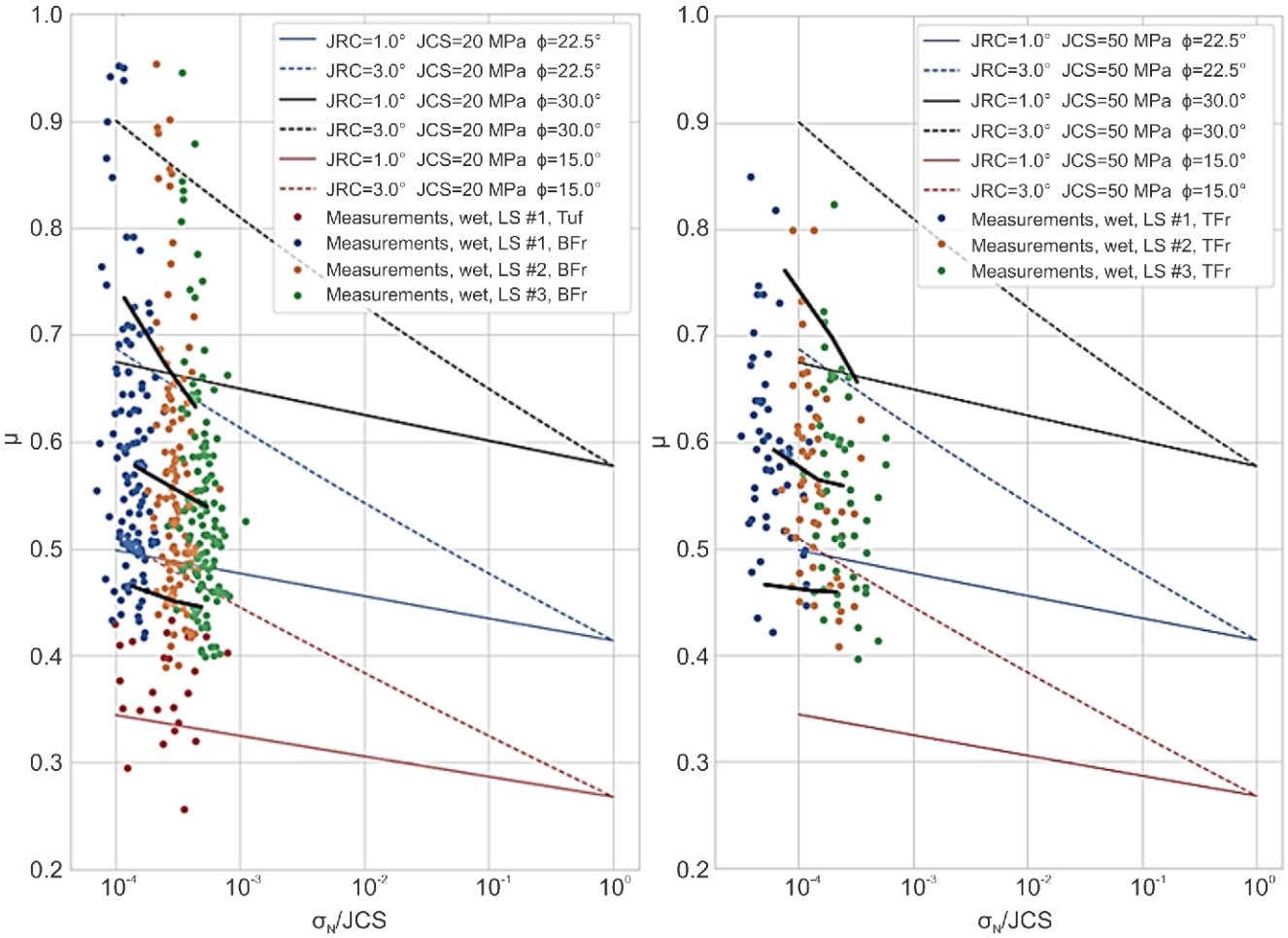

Fig. 11. Results of μ measurements with Barton's function values (according to Eq. 5) for minimum and maximum values of coefficients for the cases of wet BFr (A), and wet TFr (B)

The normal stress values ($_n$) are calibrated by strength (*JCS*). Black lines link mean measured values for load steps for three groups of measurements in which μ in the first load step falls in the ranges <0.5, 0.5–0.7 and >0,7. Coloured lines shows three options of Barton's function changes for the maximum value of $_b$ = 30° (black),the mean value of $_b$ = 22.5° (blue) and minimum $_b$ = 15° (red) and options of maximum roughness *JRC* = 3 (dashed lines) and minimum *JRC* = 1 (solid lines). Measurements for load steps are distinguished by colour points. The red dots stand for tuffite/bentonite

ent on the initial shear stress at the fracture surface. The smaller the natural shear stress, the higher the hydraulic pressure that is needed for triggering the slip. E.g. the shear stress at flat-lying bedding fractures is usually close to zero due to its orthogonal position with respect to the principal stress axis. In this case, the effective normal stress during arresting of the vertical hydraulic fracture at the bedding plane can also be very low. Shear stress exerted on sub-vertical joints, common in the boreholes studied, depends on the stress regime, being the difference between principal horizontal stresses and their orientation relative to the fracture surface. The differential stress acting on the shale interval studied ranges between 10–30 MPa in a normal faulting stress regime (Piłacik and Jarosiński, 2021), in which shear stress acting on vertical fractures is close to zero. Considering the above, it is clear that the effective loads acting on the fractures analysed during fracturing would be relatively small, around 1 MPa, which we can use as a reference value for natural reservoir conditions.

If we take into account the decreasing μ trend lines determined and extrapolate them using Barton's function (Fig. 11), we can estimate the μ value decrease for a transition from experiment to reservoir conditions. The Barton diagrams shown (Fig. 11) converge at the point where $_n$ = *JCS* = 20 MPa (for BFrs) or $_n$ = *JCS* = 50 MPa (for TFrs). Thus, the reference reservoir load, $_n$ = 1 MPa, is between 10^{-2} < $_n$/*JCS* <10^{-1}. For most rough fractures a steep decreasing trend line close to that representative for *JRC* >3 indicates that the μ values determined during the tests should be lowered by >0.2 to meet the reservoir conditions. For fractures with moderate initial friction, the decreasing gradient μ would follow this characteristic for *JRC* ~ 2, that point to μ values for the reservoir ~0.1 lower than in the experiments. For the smoothest fractures with *JRC* <1 the μ reduction would be <0.05. Because these are very rough estimates, the correction values do not refer to particular load steps.

CONCLUSIONS

Multiple shear experiments were performed to determine the static friction coefficients (μ) for 118 bedding fractures (BFrs) and 52 tectonic fractures (TFrs) taken from borehole core from lower Paleozoic shales of the Baltic Basin. For each fracture, 18 measurements were made in three load steps and

in dry and wet conditions, or exceptionally more. Experiments were carried out in a self-made shear device under very low fracture-normal load ($_n$) conditions in the range of 1.5–20 kPa.

We have ensured that, under such low loads, even 18 measurement repetitions done on the same fracture do not result in fracture surface wear that would result in systematic deviation of the μ value. The precision of measurements on the same fracture and conditions is determined at ±2.2% on average.

For the vast majority of fractures, it was found that as the normal load increases, the measured μ value decreases, which for the difference between the first and third load steps exceeds the precision of the measurements.

A significant decrease in μ value also occurred due to wetting of the fracture surface, which resulted in a decrease of the friction angle (or basic friction angle $_b$) by an average of 10% for BFrs and 4% for TFrs, exceeding significantly the precision of our measurements.

The decreasing μ value trends measured are comparable to those predicted by Barton's function in a realistic range of parameters: joint roughness coefficient *JRC* (1–3), joint strength coefficient *JCS* (20–50 MPa) and $_b$ (15–30°). Some exceptions are represented by the fractures with the highest μ, for which we suspect slip blocking by major irregularities, and the fractures with the lowest μ values, represented by BFrs covered by bentonite/tuffite, for which lower JRC and $_b$ are needed.

Following the μ decrease predicted by Barton's formula it was estimated that, in the use of the test results obtained under low loads for reservoir applications, the measured μ values require a reduction by ~0.05 to 0.2. A larger correction is needed for a higher initial μ value.

The method we present is characterized by its simplicity and the possibility of carrying out analyses under core storage conditions, e.g. accompanied by any core profiling. Its statistical results, which show a significant variation of friction coefficient values in shales, can be applied to geomechanical models of fractured reservoirs. However, the conversion of the coefficient of friction to reservoir conditions is temporarily hypothetical, and seems worth refining when the observations are supplemented with at least one of the additional parameters of the empirical Barton function.

Acknowledgements. We are grateful to the Polish Oil and Gas Company for allowing us to perform friction experiments on their borehole core and to Kinga Bobek from the Polish Geological Institute for her help in field experiments. The research was supported by the Polish National Centre for Research and Development (grant BG2/SHALEMECH/14), National Science Centre (project 2019/33/N/ST10/00473) and the Polish Geological Institute-NRI (project 61.8609.1702.00.0).

REFERENCES

Aimene, Y.E., Ouenes, A., 2015. Geomechanical modeling of hydraulic fractures interacting with natural fractures – validation with microseismic data and tracer data from the Marcellus and Eagle Ford. Interpretation, **3**: SU71–SU88; https://doi.org/10.1190/INT-2014-0274.1

Amontons, M., 1699. De la resistance causée dans les machines. Memoir de l'Academie Royale des Sciences: 206–227. Amsterdam.

Anderson, G.D., 1981. Effects of friction on hydraulic fracture growth near unbounded interfaces in rocks. SPE Journal, **21**: 21–29; https://doi.org/10.2118/8347-PA

Bachmann, C.E., Wiemer, S., Goertz-Allmann, B.P., Woessner, J., 2012. Influence of pore-pressure on the event-size distribution of induced earthquakes. Geophysical Research Letters, **39**, L09302; https://doi.org/10.1029/2012GL051480

Bandis, S., Lumsden, A.C., Barton, N., 1981. Experimental studies of scale effects on the shear behaviour of rock joints. International Journal of Rock Mechanics and Mining Sciences & Geomechanics Abstracts, **18**: 1–21; https://doi.org/10.1016/0148-9062(81)90262-X

Barton, N., 1973. Review of a new shear strength criterion for rock joints. Engineering Geology, **7**: 287–332; https://doi.org/10.1016/0013-7952(73)90013-6

Barton, N., 1976. The Shear Strength of Rock and Rock Joints. International Journal of Rock Mechanics and Mining Sciences & Geomechanics Abstracts, **13**: 255–279; https://doi.org/10.1016/0148-9062(76)90003-6

Barton, N., 2013. Shear strength criteria for rock, rock joints, rockfill and rock masses: Problems and some solutions, Journal of Rock Mechanics and Geotechnical Engineering, **5**: 249–261; https://doi.org/10.1016/j.jrmge.2013.05.008

Barton, N., Choubey, V., 1977. The shear strength of joints in theory and practice. Rock Mechanics and Rock Engineering, **10**: 1–54; https://doi.org/10.1007/BF01261801

Bobek, K., Jarosiński, M., 2018. Parallel structural interpretation of drill cores and microresistivity scanner images from gas-bearing shale (Baltic Basin, Poland). Interpretation, **6**: SH25–SH38; https://doi.org/10.1190/INT-2017-0211.1

Bobek, K., Jarosiński, M., 2021. Modifications of methods for the fracture analysis from borehole data in application to shale formations. Geological Quarterly, **65** (2), 23; https://doi.org/10.7306/gq.1590

Cawsey, D.C., Farrar, N.S., 1976. Discussion: a simple sliding apparatus for the measurement of rock joint friction. Géotechnique, **26**: 641–644; https://doi.org/10.1680/geot.1976.26.4.641

Cooke, M.L., Underwood, C.A., 2001. Fracture termination and step-over at bedding interfaces due to frictional slip and interface opening. Journal of Structural Geology, **23**: 223–228; https://doi.org/10.1016/S0191-8141(00)00092-4

Engelder, T., Lash, G.G., Uzcátegui, R.S., 2009. Joint sets that enhance production from Middle and Upper Devonian gas shales of the Appalachian Basin. AAPG Bulletin, **93**: 857–889; https://doi.org/10.1306/03230908032

Eshiet, K.I., Sheng, Y., 2017. The role of rock joint frictional strength in the containment of fracture propagation. Acta Geotechnica, **12**: 897–920; https://doi.org/10.1007/s11440-016-0512-2

Gale, J.F., Laubach, W.S.E., Olson, J.E., Eichhubl, P., Fall A., 2014. Natural fractures in shale: a review and new observations. AAPG Bulletin, **98**: 2165–2216; https://doi.org/10.1306/08121413151

Gu, M., Kulkarni, P., Rafiee, M., Ivarrud, E., Mohanty, K., 2016. Optimum fracture conductivity for naturally fractured shale and tight reservoirs. SPE Production & Operators, **31**: 289–299; https://doi.org/10.2118/171648-PA

Gutierrez, M., Øino, L.E., Høeg, K., 2000. The effect of fluid content on the mechanical behaviour of fractures in chalk. Rock Mechanics and Rock Engineering, **33**: 93–117; https://doi.org/10.1007/s006030050037

Hu, X.Q., Cruden, D.M., 1988. Basic friction angles of carbonate rocks from Kananaskis country, Canada. Bulletin of the International Association of Engineering Geology, **38**: 55–59; https://doi.org/10.7939/R3DW1X

ISRM, 2007. The complete ISRM suggested methods for rock characterization, testing and monitoring: 1974–2006. In: Suggested Methods Prepared by the Commission on Testing Methods, ISRM (eds. R. Ulusay and J.A. Hudson). Compilation arranged by the ISRM Turkish National Group, Kozan Ofset, Ankara.

ISRM, 2015. The ISRM Suggested Methods for Rock Characterization, Testing and Monitoring: 2007–2014 (ed. R. Ulusay); https://doi.org/10.1007/978-3-319-07713-0

Jaeger, J.C., Cook, N.G., 1979. Fundamentals of Rock Mechanics. 3rd edition. Chapman and Hall, London; https://doi.org/10.1017/S001675680003274X

Jumikis, A.R., 1966. Some Engineering Aspects of Brunswick Shale. Proceedings of the 1st Congress of the International Society for Rock Mechanics. Lisbon, Portugal

Kulander, B.R., Dean, S.L., Ward Jr., B.J., 1990. Induced fractures in core. AAPG Methods in Exploration, **8**: 25–57; https://doi.org/10.1306/Mth8516

Liu, H.L., Wang, H.Y., Liu, R.H., Zhao, Q., Lin, Y.J., 2010. China shale gas resources and prospect potential (in Chinese with English summary). Acta Geologica Sinica, **84**: 1374–1378.

Lorenz, J.C., Cooper, S.P., 2017. Atlas of Natural and Induced Fractures in Core. Wiley.

Maxwell, S.C., 2011. What does microseismic tell us about hydraulic fracture deformation. Recorder, **36**: 30–45; https://doi.org/10.1190/1.362750

Muralha, J., Grasselli, G., Tatone, B., Blümel, M., Chryssanthakis, P., Yujing, J., 2014. ISRM suggested method for laboratory determination of the shear strength of rock joints: revised version. Rock Mechanics and Rock Engineering, **47**: 291–302; https://doi.org/10.1007/s00603-013-0519-z

Pearson, K., 1895. Note on regression and inheritance in the case of two parents. Proceedings of the Royal Society of London, **58**: 240–242; https://doi.org/10.1098/rspl.1895.0041

Piłacik, A., Jarosiński, M., 2021. Present-day stress profile in the Baltic Basin sedimentary succession constrained by drilling-induced structures: interpretation uncertainties. Geological Quarterly, **65** (4), 51; https://doi.org/10.7306/gq.1620

Podhalańska, T., Feldman-Olszewska, A., Roszkowska-Remin, J., Janas, M., Pachytel, R., Głuszyński, A., Roman, M., 2020. Prospective zones of unconventional hydrocarbon reservoirs in the Cambrian, Ordovician and Silurian shale formations of the East European Craton marginal zone in Poland. Geological Quarterly, **64** (2): 342–376; https://doi.org/10.7306/gq.1540

Poprawa, P., 2020. Lower Paleozoic oil and gas shale in the Baltic-Podlasie-Lublin Basin (central and eastern Europe) – a review. Geological Quarterly, **64** (3): 515–566; https://doi.org/10.7306/gq.1542

Ramsay, J.G., Huber, M.I., 1987. Techniques in Modern Structural Geology. **2**: Folds and Fractures. London Academic Press.

Renshaw, C.E., Pollard, D.D., 1995. An experimentally verified criterion for propagation across unbounded frictional interfaces in brittle, linear elastic materials. International Journal of Rock Mechanics and Mining Sciences & Geomechanics Abstracts, **32**: 237–249; https://doi.org/10.1016/0148-9062(94)00037-4

Wojtowicz, M., Jarosiński, M., Pachytel, R., 2021. Unconfined compressive strength of Lower Paleozoic shales from the Baltic Basin (northern Poland). Geological Quarterly, **65** (2), 33; https://doi.org/10.7306/gq.1603

Yan, X., You, L., Kang, Y., Li, X., Xu, C., She, J., 2018. Impact of drilling fluids on friction coefficient of brittle gas shale. International Journal of Rock Mechanics and Mining Sciences, **106**: 144–152; https://doi.org/10.1016/j.ijrmms.2018.04.026

You, L.J., Kang, Y.L., Chen, Z.X., Chen, Q., Yang, B., 2014. Wellbore instability in shale gas wells drilled by oil-based fluids. International Journal of Rock Mechanics and Mining Sciences, **72**: 294–299; https://doi.org/10.1016/j.ijrmms.2014.08.017

Zoback, M.D., Barton, C.A. , Brudy, M., Castillo, D.A., Finkbeiner, T., Grollimund, B.R., Moss, D.B., Peska, P., Ward, C.D., Wiprut, D.J., 2003. Determination of stress orientation and magnitude in deep wells. International Journal of Rock Mechanics and Mining Sciences, **40**: 1049–1076; https://doi.org/10.1016/j.ijrmms.2003.07.001

APPENDIX 1

No	Depth [m]	Formation	Type	σ1 [kPa]	μ11	μ12	μ13	σ2 [kPa]	μ21	μ22	μ23	σ3 [kPa]	μ31	μ32	μ33	σ4 [kPa]	μ41	μ42	μ43	σ5 [kPa]	μ51	μ52	μ53	σ6 [kPa]	μ61	μ62	μ63
1	3709,44	Sasino	Tf	4,428	0,473	0,460	0,484	12,245	0,401	0,407	0,398	N/A	N/A	N/A	N/A	4,428	0,399	0,412	0,417	12,245	0,385	0,410	0,384	N/A	N/A	N/A	N/A
2	3706,24	Sasino	Tf	3,502	0,478	0,494	0,493	9,998	0,384	0,381	0,379	N/A	N/A	N/A	N/A	3,502	0,405	0,391	0,398	9,998	0,417	0,423	0,421	N/A	N/A	N/A	N/A
3	3704,03	Sasino	BFr	2,256	1,013	0,969	0,999	5,406	1,054	1,032	1,066	8,555	0,959	0,976	0,981	2,256	1,000	1,013	0,997	5,406	0,933	0,895	0,875	8,555	0,880	0,890	0,867292472
4	3711,73	Sasino	TFr	2,146	0,703	0,666	0,648	5,018	0,611	0,591	0,584	7,891	0,555	0,541	0,529	2,146	0,420	0,442	0,444	5,018	0,449	0,450	0,454	7,891	0,475	0,484	0,487986895
5	3700,56	Sasino	BFr	2,984	0,947	0,945	0,907	6,287	0,947	0,955	0,938	9,590	0,879	0,880	0,879	2,984	0,497	0,525	0,497	6,287	0,541	0,546	0,525	9,590	0,562	0,549	0,55433098
6	3712,34	Sasino	BFr	2,512	0,526	0,531	0,533	5,815	0,514	0,523	0,522	9,118	0,513	0,499	0,513	2,512	0,463	0,464	0,472	5,815	0,412	0,432	0,415	9,118	0,429	0,433	0,437058504
7	3223,25	Sasino	BFr	2,467	0,594	0,611	0,598	5,770	0,616	0,626	0,614	10,725	0,581	0,599	0,601	2,467	0,488	0,513	0,516	5,770	0,489	0,487	0,487	10,725	0,448	0,457	0,456267324
8	3224,93	Sasino	BFr	2,413	0,919	0,860	0,867	5,716	0,859	0,873	0,869	9,019	0,869	0,876	0,870	2,413	0,817	0,761	0,797	5,716	0,788	0,788	0,782	9,019	0,780	0,774	0,772019777
9	3230,36	Sasino	Tf	1,977	0,464	0,449	0,442	5,280	0,458	0,450	0,443	8,583	0,427	0,436	0,433	1,977	0,423	0,431	0,435	5,280	0,390	0,405	0,398	8,583	0,393	0,381	0,38426015
10	3234,93	Sasino	TFr	2,009	0,703	0,699	0,694	5,345	0,689	0,667	0,668	8,682	0,634	0,646	0,644	2,009	0,616	0,628	0,634	5,345	0,592	0,578	0,604	8,682	0,575	0,570	0,564373559
11	3234,93	Sasino	TFr	2,009	0,744	0,752	0,757	5,345	0,723	0,734	0,735	8,682	0,691	0,685	0,678	2,009	0,724	0,682	0,703	5,345	0,657	0,667	0,668	8,682	0,597	0,614	0,607993851
12	2935,58	Sasino	Tf	2,730	0,500	0,486	0,492	5,152	0,493	0,485	0,484	7,574	0,500	0,491	0,485	2,730	0,409	0,410	0,422	5,152	0,424	0,427	0,415	7,574	0,425	0,414	0,415414135
13	2933,68	Sasino	Tf	5,632	0,474	0,467	0,469	10,630	0,481	0,478	0,480	15,627	0,469	0,475	0,470	5,632	0,413	0,445	0,441	10,630	0,421	0,421	0,411	15,627	0,408	0,402	0,399424368
14	2928,87	Sasino	BFr	2,943	0,692	0,697	0,676	7,632	0,650	0,633	0,641	12,321	0,614	0,621	0,624	2,943	0,571	0,589	0,578	7,632	0,551	0,544	0,554	12,321	0,550	0,532	0,548430067
15	2917,20	Sasino	BFr	4,899	0,592	0,613	0,619	13,553	0,602	0,580	0,577	22,208	0,548	0,557	0,560	4,899	0,644	0,628	0,613	13,553	0,563	0,549	0,558	22,208	0,521	0,527	0,530007794
16	2930,74	Sasino	TFr	3,345	0,551	0,552	0,544	8,684	0,527	0,569	0,562	14,022	0,491	0,478	0,475	3,345	0,621	0,598	0,584	8,684	0,541	0,539	0,529	14,022	0,550	0,560	0,556063202
17	2930,74	Sasino	TFr	3,345	0,605	0,619	0,630	8,684	0,552	0,551	0,542	14,022	0,492	0,501	0,485	3,345	0,729	0,735	0,728	8,684	0,635	0,652	0,634	14,022	0,534	0,543	0,551684752
18	2915,52	Sasino	TFr	2,688	0,582	0,613	0,591	7,274	0,531	0,544	0,526	11,860	0,463	0,466	0,458	2,688	0,615	0,579	0,561	7,274	0,552	0,562	0,565	11,860	0,512	0,510	0,511407579
19	2915,52	Sasino	TFr	2,688	0,575	0,568	0,563	7,274	0,508	0,507	0,509	11,860	0,464	0,449	0,457	2,688	0,602	0,652	0,639	7,274	0,515	0,514	0,541	11,860	0,510	0,503	0,500966744
20	2898,74	Sasino	Tf	3,480	0,612	0,564	0,582	7,792	0,449	0,451	0,442	N/A	N/A	N/A	N/A	3,480	0,327	0,305	0,325	7,792	0,353	0,333	0,336	N/A	N/A	N/A	N/A
21	2912,35	Sasino	BFr	2,276	0,788	0,800	0,830	5,162	0,791	0,775	0,788	8,047	0,788	0,798	0,783	2,276	0,692	0,701	0,723	5,162	0,683	0,676	0,660	8,047	0,636	0,644	0,645930441
22	2920,50	Sasino	Tf	2,144	0,538	0,541	0,557	4,856	0,533	0,537	0,528	7,567	0,480	0,472	0,481	2,144	0,371	0,376	0,385	4,856	0,392	0,412	0,391	7,567	0,373	0,365	0,358179538
23	2920,20	Sasino	BFr	1,912	0,825	0,851	0,792	4,411	0,846	0,803	0,835	6,911	0,768	0,820	0,828	1,912	0,602	0,590	0,630	4,411	0,872	0,904	0,889	6,911	0,838	0,807	0,837432188
24	2905,80	Sasino	TFr	2,116	0,789	0,745	0,787	4,849	0,760	0,744	0,742	7,582	0,759	0,761	0,746	2,116	0,585	0,594	0,602	4,849	0,597	0,623	0,624	7,582	0,616	0,612	0,618781543
25	2906,90	Sasino	TFr	2,663	0,737	0,693	0,729	7,000	0,650	0,681	0,702	13,505	0,699	0,705	0,687	2,663	0,658	0,688	0,702	7,000	0,636	0,652	0,650	13,505	0,657	0,669	0,655587669
26	2906,90	Sasino	TFr	2,663	0,722	0,693	0,700	7,000	0,727	0,759	0,746	13,505	0,689	0,678	0,685	2,663	0,609	0,590	0,617	7,000	0,616	0,619	0,636	13,505	0,657	0,637	0,634952978
27	2908,78	Sasino	TFr	2,201	0,685	0,715	0,724	5,259	0,667	0,691	0,663	8,316	0,612	0,620	0,616	2,201	0,767	0,748	0,726	5,259	0,719	0,735	0,745	8,316	0,699	0,717	0,723345588
28	2908,78	Sasino	TFr	2,201	0,606	0,624	0,626	5,259	0,593	0,583	0,565	8,316	0,569	0,567	0,599	2,201	0,640	0,623	0,653	5,259	0,672	0,679	0,681	8,316	0,699	0,675	0,694117647
29	2909,45	Sasino	TFr	2,830	0,763	0,703	0,730	7,279	0,685	0,715	0,684	11,728	0,698	0,682	0,692	2,830	0,550	0,578	0,594	7,279	0,611	0,619	0,635	11,728	0,666	0,677	0,662556904
30	2915,79	Sasino	TFr	1,962	0,653	0,701	0,718	4,869	0,733	0,693	0,727	7,775	0,684	0,678	0,675	1,962	0,684	0,641	0,715	4,869	0,606	0,608	0,612	7,775	0,537	0,537	0,54635514
31	2915,79	Sasino	TFr	2,938	0,697	0,705	0,675	8,328	0,669	0,677	0,672	N/A	N/A	N/A	N/A	2,938	0,671	0,707	0,681	8,328	0,605	0,620	0,637	N/A	N/A	N/A	N/A
32	2902,00	Sasino	BFr	2,177	0,449	0,414	0,414	4,676	0,465	0,457	0,463	8,425	0,500	0,490	0,496	2,177	0,451	0,449	0,417	4,676	0,492	0,498	0,487	8,425	0,544	0,543	0,524770098
33	2859,28	Sasino	TFr	5,268	0,672	0,650	0,666	14,062	0,591	0,588	0,575	N/A	N/A	N/A	N/A	5,268	0,487	0,503	0,492	14,062	0,482	0,474	0,510	N/A	N/A	N/A	N/A
34	2861,10	Sasino	TFr	3,125	0,754	0,793	0,795	6,700	0,802	0,806	0,811	10,275	0,781	0,787	0,793	3,125	0,828	0,808	0,816	6,700	0,796	0,815	0,786	10,275	0,655	0,673	0,655532359
35	2849,57	Sasino	BFr	3,349	0,606	0,609	0,632	5,849	0,551	0,559	0,542	8,348	0,517	0,528	0,541	3,349	0,408	0,426	0,416	5,849	0,455	0,477	0,454	8,348	0,449	0,437	0,449700599
36	2853,93	Sasino	BFr	3,135	0,982	0,962	0,995	5,635	1,001	1,038	1,051	6,884	0,990	0,985	0,976	3,135	0,765	0,789	0,782	5,635	0,863	0,870	0,820	6,884	0,829	0,834	0,841168996
37	2865,80	Sasino	Tf	2,152	0,453	0,438	0,433	3,958	0,447	0,464	0,450	5,765	0,436	0,435	0,427	2,152	0,416	0,407	0,406	3,958	0,360	0,371	0,368	5,765	0,352	0,353	0,349106863
38	2866,75	Sasino	BFr	2,038	0,646	0,660	0,653	3,615	0,587	0,597	0,592	5,192	0,576	0,565	0,568	2,038	0,590	0,564	0,602	3,615	0,548	0,561	0,555	5,192	0,527	0,518	0,519744836
39	2866,70	Sasino	BFr	3,363	0,619	0,608	0,613	8,035	0,590	0,593	0,581	15,042	0,592	0,600	0,603	3,363	0,583	0,581	0,568	8,035	0,556	0,537	0,562	15,042	0,509	0,523	0,504347826
40	3959,50	Sasino	BFr	2,099	0,821	0,815	0,795	5,248	0,879	0,853	0,860	9,972	0,847	0,859	0,822	2,099	0,688	0,684	0,701	5,248	0,720	0,748	0,746	9,972	0,749	0,744	0,757776725
41	3961,97	Sasino	BFr	1,932	0,425	0,441	0,434	5,081	0,449	0,423	0,437	9,805	0,434	0,440	0,433	1,932	0,457	0,447	0,477	5,081	0,438	0,457	0,444	9,805	0,422	0,447	0,410791714
42	3965,16	Sasino	TFr	3,130	0,492	0,461	0,468	7,539	0,524	0,523	0,533	14,153	0,488	0,502	0,513	3,130	0,551	0,553	0,558	7,539	0,534	0,566	0,561	14,153	0,605	0,589	0,603271028
43	3972,18	Sasino	TFr	1,809	0,609	0,653	0,616	3,865	0,623	0,644	0,628	6,950	0,568	0,565	0,586	1,809	0,545	0,489	0,537	3,865	0,520	0,508	0,523	6,950	0,522	0,507	0,508803077
44	3967,25	Sasino	Tf	6,389	0,413	0,419	0,415	12,520	0,395	0,400	0,431	N/A	N/A	N/A	N/A	6,389	0,315	0,343	0,374	12,520	0,361	0,353	0,352	N/A	N/A	N/A	N/A
45	3552,88	Pelplin	BFr	3,099	0,541	0,563	0,564	6,248	0,544	0,564	0,545	10,972	0,513	0,530	0,529	3,099	0,515	0,543	0,563	6,248	0,532	0,524	0,510	10,972	0,492	0,481	0,469001148
46	3552,81	Pelplin	BFr	3,346	0,640	0,661	0,666	6,495	0,727	0,749	0,552	11,219	0,742	0,748	0,771	3,346	0,631	0,576	0,601	6,495	0,544	0,595	0,646	11,219	0,586	0,562	0,591157895
47	3553,18	Pelplin	BFr	2,680	0,476	0,503	0,505	7,060	0,493	0,470	0,489	N/A	N/A	N/A	N/A	2,680	0,405	0,359	0,395	7,060	0,377	0,350	0,380	N/A	N/A	N/A	N/A

48	3556,73	Pelplin	BFr	2,543	0,597	0,626	0,663	5,692	0,667	0,672	0,676	10,416	0,655	0,669	0,676	2,543	0,623	0,643	0,614	5,692	0,576	0,601	0,594	10,416	0,601	0,607	0,590929705
49	3565,38	Pelplin	TFr	1,895	0,625	0,706	0,654	4,430	0,663	0,635	0,612	8,232	0,656	0,671	0,656	1,895	0,632	0,724	0,660	4,430	0,647	0,710	0,605	8,232	0,592	0,584	0,593379523
50	3565,38	Pelplin	TFr	1,895	0,674	0,584	0,615	4,430	0,642	0,639	0,638	8,232	0,667	0,676	0,646	1,895	0,960	0,744	0,845	4,430	0,812	0,755	0,829	8,232	0,716	0,739	0,712702079
51	3574,25	Pelplin	BFr	2,288	0,961	1,015	1,002	5,437	0,926	0,961	0,933	8,587	0,931	0,943	0,971	2,288	0,937	0,942	0,970	5,437	0,870	0,828	0,820	10,161	0,744	0,713	0,748953975
52	3577,33	Pelplin	TFr	2,426	0,635	0,576	0,646	5,320	0,577	0,628	0,602	9,661	0,614	0,625	0,616	2,426	0,627	0,584	0,593	5,320	0,614	0,605	0,594	9,661	0,607	0,601	0,607757975
53	3599,57	Pelplin	TFr	2,180	0,737	0,796	0,704	5,345	0,746	0,720	0,766	10,092	0,706	0,694	0,700	2,180	0,671	0,747	0,798	5,345	0,696	0,711	0,725	10,092	0,815	0,798	0,857322045
54	3624,21	Pelplin	Tf	1,802	0,459	0,475	0,463	5,110	0,453	0,461	0,457	N/A	N/A	N/A	N/A	1,802	0,447	0,444	0,451	5,110	0,444	0,435	0,437	N/A	N/A	N/A	N/A
55	3617,94	Pelplin	BFr	2,759	0,753	0,787	0,772	5,908	0,934	0,943	0,960	9,057	0,812	0,803	0,812	2,759	0,843	0,740	0,793	5,908	0,554	0,564	0,570	9,057	0,640	0,658	0,640646732
56	3610,55	Pelplin	BFr	2,601	0,789	0,788	0,803	5,751	0,825	0,837	0,842	8,900	0,810	0,793	0,782	2,601	0,686	0,722	0,665	5,751	0,626	0,634	0,629	8,900	0,559	0,559	0,546001415
57	3614,62	Pelplin	TFr	2,545	0,684	0,675	0,707	5,988	0,705	0,702	0,677	9,430	0,731	0,724	0,693	2,545	0,659	0,630	0,674	5,988	0,645	0,673	0,643	9,430	0,637	0,681	0,659791933
58	3615,05	Pelplin	TFr	1,561	0,637	0,630	0,639	3,513	0,614	0,627	0,644	5,465	0,618	0,609	0,599	1,561	0,590	0,605	0,622	3,513	0,556	0,531	0,581	5,465	0,574	0,577	0,562243258
59	3608,00	Pelplin	TFr	2,062	0,619	0,634	0,659	5,127	0,597	0,567	0,581	8,193	0,644	0,639	0,625	2,062	0,640	0,629	0,647	5,127	0,565	0,550	0,566	8,193	0,666	0,644	0,641347053
60	3601,65	Pelplin	TFr	1,917	0,574	0,607	0,620	4,635	0,588	0,622	0,621	7,352	0,571	0,590	0,581	1,917	0,534	0,531	0,519	4,635	0,527	0,495	0,509	7,352	0,522	0,545	0,553132508
61	3600,05	Pelplin	TFr	2,285	0,470	0,458	0,479	5,449	0,492	0,459	0,477	8,614	0,518	0,534	0,492	2,285	0,478	0,479	0,507	5,449	0,553	0,558	0,582	8,614	0,560	0,549	0,556943424
62	3133,57	Pelplin	Tf	3,136	0,343	0,351	0,345	5,931	0,320	0,331	0,330	8,726	0,321	0,307	0,313	3,136	0,358	0,354	0,334	5,931	0,331	0,332	0,327	8,726	0,320	0,318	0,321588725
63	3135,64	Pelplin	BFr	2,343	0,572	0,566	0,559	4,248	0,528	0,521	0,519	6,153	0,525	0,544	0,537	2,343	0,463	0,467	0,464	4,248	0,455	0,458	0,467	6,153	0,455	0,441	0,43498452
64	3126,85	Pelplin	Tf	2,279	0,377	0,389	0,400	4,310	0,392	0,388	0,380	6,341	0,353	0,355	0,357	2,279	0,343	0,349	0,359	4,310	0,355	0,345	0,350	6,341	0,332	0,338	0,342408712
65	3094,96	Pelplin	BFr	2,400	0,539	0,536	0,534	5,703	0,535	0,538	0,539	9,006	0,514	0,508	0,516	2,400	0,580	0,600	0,588	5,703	0,522	0,520	0,525	9,006	0,494	0,493	0,486704566
66	3095,84	Pelplin	BFr	2,495	0,487	0,490	0,491	5,798	0,479	0,466	0,465	9,102	0,463	0,471	0,468	2,495	0,478	0,529	0,529	5,798	0,488	0,510	0,508	9,102	0,471	0,474	0,47849755
67	3110,49	Pelplin	BFr	3,823	0,623	0,645	0,642	7,126	0,608	0,624	0,631	10,429	0,629	0,628	0,616	3,823	0,614	0,603	0,616	7,126	0,571	0,582	0,585	10,429	0,563	0,571	0,558036421
68	2847,50	Pelplin	TFr	4,083	0,537	0,571	0,535	11,560	0,475	0,476	0,476	19,037	0,441	0,433	0,434	4,083	0,560	0,629	0,594	11,560	0,463	0,459	0,475	19,037	0,466	0,464	0,461508248
69	2847,50	Pelplin	TFr	4,083	0,525	0,497	0,504	11,560	0,402	0,388	0,391	19,037	0,395	0,393	0,392	4,083	0,601	0,581	0,586	11,560	0,430	0,439	0,456	19,037	0,458	0,464	0,453652789
70	2845,20	Pelplin	TFr	6,140	0,709	0,686	0,657	17,416	0,659	0,660	0,671	28,691	0,637	0,628	0,625	6,140	0,637	0,624	0,635	17,416	0,612	0,626	0,624	28,691	0,593	0,609	0,609746512
71	2845,20	Pelplin	TFr	6,140	0,629	0,637	0,643	17,416	0,617	0,626	0,624	28,691	0,600	0,589	0,597	6,140	0,583	0,595	0,624	17,416	0,579	0,583	0,594	28,691	0,582	0,576	0,577716644
72	2847,90	Pelplin	BFr	3,020	0,590	0,620	0,608	7,585	0,610	0,605	0,601	12,150	0,573	0,570	0,577	3,020	0,491	0,502	0,489	7,585	0,489	0,509	0,494	12,150	0,486	0,483	0,480931805
73	2842,32	Pelplin	BFr	3,095	0,819	0,769	0,777	7,660	0,727	0,749	0,741	12,225	0,727	0,715	0,712	3,095	0,673	0,712	0,718	7,660	0,679	0,692	0,694	12,225	0,648	0,652	0,647684839
74	2840,80	Pelplin	BFr	3,835	0,576	0,577	0,563	8,399	0,579	0,583	0,587	15,247	0,580	0,581	0,582	3,835	0,500	0,513	0,510	8,399	0,497	0,501	0,497	15,247	0,457	0,457	0,461676647
75	2837,80	Pelplin	BFr	3,417	0,625	0,597	0,603	7,982	0,632	0,625	0,621	12,547	0,605	0,594	0,586	3,417	0,533	0,573	0,547	7,982	0,538	0,553	0,544	12,547	0,529	0,523	0,527560488
76	2832,23	Pelplin	BFr	3,184	0,573	0,599	0,582	7,749	0,583	0,575	0,568	12,314	0,585	0,574	0,573	3,184	0,505	0,500	0,495	7,749	0,481	0,487	0,486	12,314	0,458	0,460	0,461909175
77	2831,70	Pelplin	BFr	3,232	0,682	0,648	0,652	7,797	0,621	0,642	0,626	12,362	0,599	0,593	0,600	3,232	0,534	0,556	0,544	7,797	0,538	0,541	0,544	12,362	0,547	0,546	0,537296898
78	2824,23	Pelplin	BFr	2,938	0,676	0,696	0,684	7,502	0,638	0,632	0,633	12,067	0,645	0,642	0,637	2,938	0,544	0,606	0,584	7,502	0,524	0,551	0,543	12,067	0,518	0,506	0,508795158
79	2820,31	Pelplin	BFr	2,714	0,615	0,644	0,583	7,535	0,559	0,583	0,579	12,355	0,564	0,553	0,550	2,714	0,520	0,567	0,571	7,535	0,482	0,499	0,506	12,355	0,484	0,489	0,493367148
80	2819,34	Pelplin	BFr	3,237	0,540	0,537	0,533	8,058	0,495	0,502	0,503	12,878	0,506	0,500	0,513	3,237	0,493	0,496	0,499	8,058	0,484	0,485	0,493	12,878	0,444	0,455	0,454800674
81	2818,54	Pelplin	BFr	4,208	0,487	0,483	0,476	9,029	0,438	0,443	0,444	16,260	0,384	0,387	0,389	4,208	0,499	0,510	0,510	9,029	0,478	0,489	0,474	16,260	0,456	0,451	0,459086866
82	2816,38	Pelplin	BFr	3,717	0,530	0,524	0,527	8,537	0,529	0,542	0,543	13,358	0,518	0,510	0,503	3,717	0,534	0,523	0,547	8,537	0,488	0,476	0,477	13,358	0,451	0,461	0,462648863
83	2803,39	Pelplin	BFr	3,659	0,722	0,767	0,738	8,480	0,777	0,759	0,756	15,710	0,735	0,731	0,725	3,659	0,728	0,750	0,711	8,480	0,712	0,727	0,713	15,710	0,663	0,660	0,664314207
84	2802,44	Pelplin	BFr	4,218	0,573	0,570	0,568	8,783	0,554	0,545	0,534	13,348	0,525	0,535	0,532	4,218	0,497	0,509	0,515	8,783	0,496	0,494	0,491	13,348	0,460	0,469	0,464603283
85	2763,78	Pelplin	BFr	1,687	0,932	0,907	0,911	4,186	0,836	0,839	0,773	6,686	0,812	0,789	0,792	1,687	0,896	0,853	0,848	4,186	0,733	0,689	0,715	6,686	0,627	0,636	0,631588785
86	2770,47	Pelplin	BFr	3,260	0,669	0,678	0,691	5,760	0,685	0,691	0,678	8,259	0,674	0,692	0,681	3,260	0,664	0,657	0,642	5,760	0,613	0,618	0,626	8,259	0,564	0,592	0,600847329
87	2774,20	Pelplin	BFr	1,951	0,629	0,618	0,635	4,450	0,604	0,600	0,616	8,199	0,682	0,676	0,680	1,951	0,625	0,630	0,625	4,450	0,555	0,549	0,540	8,199	0,518	0,531	0,528120713
88	3817,05	Pelplin	TFr	2,427	0,639	0,657	0,649	5,576	0,565	0,559	0,595	10,300	0,577	0,577	0,567	2,427	0,760	0,762	0,694	5,576	0,515	0,563	0,561	10,300	0,526	0,524	0,526983642
89	3843,52	Pelplin	BFr	3,716	0,718	0,695	0,714	6,865	0,675	0,702	0,653	11,589	0,618	0,639	0,635	3,716	0,698	0,692	0,721	6,865	0,657	0,631	0,605	11,589	0,585	0,563	0,558152174
90	3850,29	Pelplin	BFr	2,952	0,557	0,514	0,531	6,102	0,523	0,512	0,518	10,826	0,554	0,542	0,521	2,952	0,612	0,594	0,591	6,102	0,577	0,556	0,572	10,826	0,521	0,514	0,5056
91	3852,85	Pelplin	BFr	2,105	0,807	0,726	0,812	5,255	0,791	0,749	0,763	9,978	0,686	0,734	0,719	2,105	1,016	0,892	0,946	5,255	0,653	0,651	0,647	9,978	0,670	0,672	0,640839514
92	3868,66	Pelplin	BFr	3,754	0,700	0,719	0,721	6,903	0,734	0,706	0,723	10,052	0,714	0,721	0,728	3,754	0,757	0,682	0,722	6,903	0,661	0,666	0,649	10,052	0,596	0,582	0,586622807
93	3880,93	Pelplin	BFr	3,529	0,689	0,708	0,693	6,678	0,736	0,723	0,736	9,827	0,642	0,629	0,641	3,529	0,632	0,637	0,662	6,678	0,618	0,625	0,623	9,827	0,609	0,620	0,555039257
94	3914,28	Pelplin	BFr	3,601	0,946	0,931	1,009	6,750	0,781	0,800	0,933	N/A	N/A	N/A	N/A	3,601	0,850	0,763	0,841	6,750	0,857	0,884	0,886	N/A	N/A	N/A	N/A
95	3688,23	Jantar	BFr	3,027	0,596	0,597	0,601	6,078	0,559	0,580	0,583	10,655	0,575	0,592	0,559	3,027	0,511	0,516	0,520	6,078	0,484	0,505	0,500	10,655	0,496	0,492	0,503865979
96	3684,82	Jantar	TFr	1,927	0,550	0,520	0,529	4,334	0,539	0,552	0,556	6,742	0,542	0,530	0,546	1,927	0,493	0,462	0,480	4,334	0,474	0,465	0,455	6,742	0,463	0,453	0,461881807
97	3686,62	Jantar	TFr	2,934	0,491	0,502	0,483	6,692	0,455	0,444	0,432	10,451	0,418	0,400	0,408	2,934	0,410	0,435	0,420	6,692	0,437	0,458	0,445	10,451	0,487	0,483	0,468980399

98	3685,00	Jantar	TFr	2,912	0,560	0,600	0,612	8,009	0,604	0,560	0,588	N/A	N/A	N/A	N/A	2,912	0,448	0,499	0,477	8,009	0,529	0,557	0,537	N/A	N/A	N/A	N/A
99	3685,00	Jantar	TFr	2,891	0,563	0,593	0,631	7,536	0,635	0,648	0,658	N/A	N/A	N/A	N/A	2,891	0,642	0,666	0,647	7,536	0,636	0,648	0,641	N/A	N/A	N/A	N/A
100	3682,91	Jantar	BFr	2,157	0,560	0,534	0,554	5,460	0,537	0,566	0,538	8,763	0,533	0,520	0,521	2,157	0,496	0,525	0,526	5,460	0,467	0,472	0,476	8,763	0,453	0,433	0,433283076
101	3684,96	Jantar	BFr	2,479	0,678	0,701	0,713	6,073	0,688	0,686	0,699	9,666	0,694	0,696	0,685	2,479	0,566	0,601	0,620	6,073	0,542	0,548	0,536	9,666	0,537	0,555	0,53197026
102	3688,36	Jantar	BFr	2,149	0,555	0,530	0,538	5,452	0,555	0,553	0,553	8,755	0,520	0,566	0,568	2,149	0,507	0,509	0,519	5,452	0,508	0,463	0,470	8,755	0,477	0,484	0,46953405
103	3200,82	Jantar	BFr	3,856	0,582	0,600	0,606	7,159	0,569	0,583	0,588	10,462	0,542	0,541	0,554	3,856	0,499	0,504	0,511	7,159	0,505	0,500	0,483	10,462	0,477	0,497	0,489502762
104	3203,50	Jantar	BFr	2,178	0,478	0,467	0,439	5,481	0,442	0,443	0,428	10,436	0,435	0,447	0,444	2,178	0,462	0,451	0,443	5,481	0,407	0,397	0,423	10,436	0,397	0,406	0,394840956
105	3205,94	Jantar	BFr	2,244	0,616	0,562	0,568	5,329	0,564	0,568	0,574	9,957	0,513	0,516	0,610	2,244	0,518	0,515	0,546	5,329	0,498	0,518	0,522	9,957	0,463	0,461	0,472192099
106	3207,31	Jantar	BFr	4,119	0,757	0,733	0,727	7,422	0,713	0,716	0,719	10,725	0,688	0,695	0,743	4,119	0,665	0,648	0,669	7,422	0,639	0,642	0,627	10,725	0,625	0,618	0,61302741
107	2902,84	Jantar	BFr	3,032	0,739	0,724	0,712	7,990	0,732	0,728	0,717	12,949	0,705	0,700	0,689	3,032	0,648	0,626	0,614	7,990	0,606	0,609	0,612	12,949	0,598	0,608	0,604441892
108	2902,66	Jantar	BFr	4,091	0,669	0,699	0,695	8,781	0,637	0,654	0,657	13,470	0,633	0,617	0,621	4,091	0,506	0,519	0,523	8,781	0,502	0,510	0,492	13,470	0,507	0,510	0,504960836
109	2899,95	Jantar	BFr	3,518	0,443	0,477	0,460	8,627	0,445	0,471	0,454	13,737	0,443	0,436	0,435	3,518	0,453	0,461	0,471	8,627	0,413	0,423	0,426	13,737	0,403	0,402	0,400595127
110	2898,89	Jantar	BFr	3,379	0,488	0,502	0,500	7,822	0,453	0,455	0,444	12,265	0,439	0,429	0,434	3,379	0,476	0,470	0,462	7,822	0,424	0,421	0,423	12,265	0,398	0,404	0,397572903
111	2901,12	Jantar	TFr	2,028	0,646	0,630	0,633	5,082	0,549	0,564	0,559	8,136	0,529	0,532	0,526	2,028	0,527	0,591	0,553	5,082	0,471	0,491	0,471	8,136	0,439	0,427	0,433183183
112	2901,12	Jantar	TFr	2,028	0,638	0,695	0,672	5,082	0,648	0,630	0,642	8,136	0,590	0,601	0,604	2,028	0,542	0,544	0,556	5,082	0,534	0,529	0,520	8,136	0,452	0,466	0,469219219
113	2900,70	Jantar	TFr	2,578	0,596	0,593	0,616	6,602	0,503	0,487	0,509	10,627	0,515	0,511	0,504	2,578	0,543	0,511	0,507	6,602	0,497	0,506	0,502	10,627	0,453	0,462	0,45767847
114	2900,70	Jantar	TFr	2,578	0,703	0,663	0,689	6,602	0,610	0,604	0,629	10,627	0,544	0,549	0,551	2,578	0,510	0,534	0,546	6,602	0,484	0,474	0,490	10,627	0,443	0,457	0,442340466
115	2885,85	Jantar	BFr	1,798	0,956	1,277	1,162	4,298	1,014	0,984	0,983	6,797	0,803	0,822	0,844	1,798	0,929	0,956	0,940	4,298	0,881	0,899	0,902	6,797	0,937	0,955	0,944842802
116	2880,92	Jantar	BFr	1,635	0,622	0,629	0,657	4,380	0,592	0,607	0,610	7,124	0,558	0,545	0,537	1,635	0,469	0,480	0,466	4,380	0,447	0,436	0,432	7,124	0,530	0,542	0,535246533
117	2888,20	Jantar	BFr	3,250	0,532	0,528	0,534	6,952	0,538	0,527	0,514	10,654	0,489	0,493	0,493	3,250	0,438	0,454	0,461	6,952	0,444	0,455	0,433	10,654	0,439	0,425	0,449096595
118	2877,93	Jantar	TFr	3,918	0,755	0,709	0,743	6,804	0,726	0,715	0,708	12,574	0,669	0,686	0,679	3,918	0,542	0,588	0,549	6,804	0,541	0,540	0,495	12,574	0,569	0,567	0,577787976
119	2890,35	Jantar	TFr	2,233	0,760	0,755	0,763	5,866	0,682	0,689	0,695	11,316	0,704	0,693	0,690	2,233	0,600	0,601	0,631	5,866	0,568	0,603	0,591	11,316	0,595	0,607	0,604270348
120	2831,80	Jantar	TFr	2,378	0,745	0,856	0,727	5,952	0,759	0,802	0,788	9,526	0,663	0,648	0,643	2,378	0,660	0,609	0,648	5,952	0,651	0,683	0,664	9,526	0,669	0,660	0,664415682
121	2827,83	Jantar	BFr	3,023	0,484	0,469	0,434	5,522	0,442	0,458	0,462	9,271	0,432	0,438	0,433	3,023	0,435	0,433	0,444	5,522	0,458	0,455	0,457	9,271	0,456	0,462	0,469739857
122	2837,15	Jantar	BFr	3,275	0,541	0,536	0,545	5,775	0,548	0,540	0,553	8,274	0,548	0,559	0,560	3,275	0,478	0,481	0,468	5,775	0,464	0,451	0,432	8,274	0,435	0,444	0,431203746
123	3947,88	Jantar	BFr	2,460	0,607	0,611	0,580	5,479	0,569	0,563	0,580	N/A	N/A	N/A	N/A	2,460	0,629	0,687	0,735	5,479	0,613	0,620	0,570	N/A	N/A	N/A	N/A
124	3947,42	Jantar	BFr	2,492	0,604	0,650	0,639	6,112	0,600	0,616	0,642	9,732	0,613	0,598	0,595	2,492	0,580	0,554	0,552	6,112	0,535	0,523	0,525	9,732	0,507	0,479	0,499349079
125	3665,54	Pasłęk	BFr	2,386	0,848	0,912	0,892	5,535	0,784	0,807	0,773	10,259	0,647	0,638	0,662	2,386	0,588	0,566	0,554	5,535	0,633	0,639	0,649	10,259	0,611	0,600	0,612125863
126	3658,30	Pasłęk	BFr	2,809	0,740	0,747	0,740	5,958	0,740	0,722	0,738	10,682	0,755	0,744	0,758	2,809	0,536	0,569	0,605	5,958	0,570	0,585	0,591	10,682	0,597	0,583	0,581367925
127	3651,83	Pasłęk	BFr	2,265	0,744	0,721	0,745	5,573	0,684	0,665	0,674	10,536	0,654	0,672	0,355	2,265	0,660	0,644	0,628	5,573	0,545	0,563	0,560	10,536	0,565	0,555	0,550164861
128	3648,37	Pasłęk	BFr	1,872	0,664	0,636	0,629	5,022	0,612	0,629	0,627	9,745	0,530	0,542	0,539	1,872	0,436	0,438	0,426	5,022	0,385	0,389	0,394	9,745	0,393	0,410	0,41299079
129	3643,83	Pasłęk	BFr	2,614	0,640	0,660	0,623	6,507	0,577	0,585	0,594	12,346	0,630	0,637	0,641	2,614	0,515	0,501	0,498	6,507	0,466	0,476	0,459	12,346	0,501	0,509	0,503231909
130	3638,85	Pasłęk	BFr	2,483	0,666	0,711	0,666	5,632	0,770	0,780	0,779	10,356	0,649	0,657	0,642	2,483	0,571	0,567	0,563	5,632	0,524	0,528	0,522	10,356	0,571	0,536	0,521210278
131	3677,82	Pasłęk	BFr	1,663	0,947	0,955	0,951	4,966	0,934	0,907	0,897	8,269	0,736	0,734	0,747	1,663	0,739	0,726	0,777	4,966	0,652	0,608	0,639	8,269	0,674	0,641	0,647493509
132	3150,13	Pasłęk	BFr	2,405	0,563	0,591	0,585	5,708	0,532	0,560	0,548	10,662	0,539	0,555	0,548	2,405	0,494	0,483	0,477	5,708	0,470	0,469	0,449	10,662	0,424	0,434	0,431846344
133	3152,14	Pasłęk	BFr	2,347	0,697	0,697	0,701	5,650	0,702	0,711	0,700	10,604	0,629	0,642	0,626	2,347	0,581	0,595	0,599	5,650	0,521	0,527	0,533	10,604	0,516	0,511	0,508487774
134	3152,85	Pasłęk	BFr	2,504	0,515	0,519	0,514	5,807	0,524	0,518	0,515	10,761	0,496	0,492	0,498	2,504	0,453	0,468	0,460	5,807	0,456	0,459	0,454	10,761	0,421	0,431	0,427409454
135	3153,94	Pasłęk	BFr	2,290	0,648	0,658	0,660	5,684	0,637	0,646	0,626	9,078	0,619	0,633	0,636	2,290	0,532	0,551	0,557	5,684	0,550	0,544	0,553	9,078	0,547	0,552	0,534492428
136	3156,13	Pasłęk	BFr	2,637	0,765	0,684	0,691	6,061	0,656	0,673	0,681	9,485	0,677	0,678	0,677	2,637	0,640	0,642	0,651	6,061	0,532	0,544	0,546	9,485	0,522	0,543	0,528158845
137	3165,46	Pasłęk	BFr	1,983	0,659	0,686	0,688	5,287	0,640	0,671	0,679	8,590	0,653	0,660	0,657	1,983	0,659	0,669	0,678	5,287	0,644	0,631	0,656	8,590	0,598	0,609	0,60853682
138	3173,34	Pasłęk	BFr	2,583	0,654	0,667	0,641	6,943	0,641	0,640	0,639	11,303	0,628	0,631	0,614	2,583	0,487	0,504	0,509	6,943	0,484	0,485	0,471	11,303	0,470	0,479	0,472324012
139	3176,96	Pasłęk	BFr	2,907	0,649	0,611	0,617	6,367	0,614	0,610	0,601	9,827	0,590	0,596	0,595	2,907	0,555	0,549	0,561	6,367	0,547	0,530	0,526	9,827	0,517	0,524	0,526760563
140	3177,91	Pasłęk	BFr	3,140	0,588	0,577	0,560	6,443	0,554	0,573	0,562	9,746	0,558	0,560	0,554	3,140	0,513	0,484	0,501	6,443	0,484	0,490	0,479	9,746	0,461	0,469	0,472970683
141	3182,93	Pasłęk	BFr	3,384	0,561	0,564	0,589	6,687	0,564	0,569	0,555	9,990	0,558	0,568	0,560	3,384	0,487	0,484	0,499	6,687	0,475	0,487	0,484	9,990	0,482	0,480	0,489502397
142	3191,14	Pasłęk	BFr	2,386	0,565	0,574	0,577	5,689	0,578	0,559	0,555	8,993	0,554	0,565	0,553	2,386	0,504	0,508	0,502	5,689	0,506	0,502	0,496	8,993	0,500	0,482	0,49164371
143	3195,92	Pasłęk	BFr	3,057	0,468	0,476	0,493	6,360	0,456	0,459	0,470	9,663	0,454	0,438	0,440	3,057	0,458	0,431	0,409	6,360	0,389	0,395	0,388	9,663	0,413	0,399	0,398393437
144	3154,32	Pasłęk	TFr	5,780	0,498	0,494	0,503	11,083	0,479	0,480	0,486	16,385	0,455	0,462	0,463	5,780	0,465	0,480	0,456	11,083	0,432	0,434	0,430	16,385	0,431	0,423	0,425242718
145	3154,32	Pasłęk	TFr	5,780	0,494	0,472	0,469	11,083	0,466	0,472	0,461	16,385	0,438	0,439	0,439	5,780	0,444	0,445	0,451	11,083	0,401	0,411	0,412	16,385	0,398	0,398	0,392880259
146	3154,16	Pasłęk	TFr	5,688	0,525	0,537	0,539	10,771	0,476	0,485	0,489	15,854	0,482	0,467	0,471	5,688	0,482	0,502	0,512	10,771	0,465	0,475	0,478	15,854	0,463	0,465	0,460724591
147	2894,51	Pasłęk	BFr	3,075	0,510	0,496	0,472	7,517	0,499	0,504	0,492	11,960	0,499	0,495	0,488	3,075	0,436	0,448	0,454	7,517	0,429	0,447	0,439	11,960	0,409	0,404	0,412518574

148	2887,90	Pasłęk	BFr	2,755	0,525	0,547	0,541	7,198	0,516	0,525	0,516	11,640	0,514	0,510	0,509	2,755	0,464	0,470	0,474	7,198	0,411	0,428	0,433	11,640	0,405	0,406	0,413549618
149	2880,68	Pasłęk	BFr	3,055	0,559	0,564	0,583	7,497	0,553	0,561	0,554	14,162	0,535	0,536	0,535	3,055	0,538	0,544	0,518	7,497	0,481	0,485	0,492	14,162	0,464	0,454	0,460862745
150	2862,43	Pasłęk	BFr	2,717	0,590	0,608	0,614	7,160	0,559	0,556	0,554	13,824	0,523	0,525	0,514	2,717	0,545	0,518	0,500	7,160	0,497	0,522	0,519	13,824	0,498	0,509	0,501365901
151	2859,56	Pasłęk	BFr	3,046	0,629	0,629	0,642	7,489	0,622	0,613	0,602	14,153	0,631	0,622	0,622	3,046	0,563	0,559	0,557	7,489	0,546	0,543	0,528	14,153	0,515	0,518	0,520483441
152	2855,70	Pasłęk	BFr	2,897	0,522	0,541	0,537	7,340	0,533	0,536	0,516	11,783	0,533	0,530	0,534	2,897	0,496	0,528	0,497	7,340	0,479	0,467	0,475	11,783	0,469	0,456	0,456636501
153	2872,65	Pasłęk	BFr	3,400	0,469	0,482	0,487	8,060	0,475	0,479	0,471	12,720	0,454	0,460	0,455	3,400	0,413	0,432	0,419	8,060	0,423	0,416	0,413	12,720	0,406	0,408	0,40923246
154	2865,52	Pasłęk	TFr	4,219	0,550	0,579	0,557	11,883	0,517	0,523	0,532	19,547	0,522	0,512	0,513	4,219	0,605	0,579	0,561	11,883	0,517	0,550	0,537	19,547	0,530	0,523	0,526171339
155	2865,52	Pasłęk	TFr	4,219	0,510	0,465	0,493	11,883	0,500	0,497	0,482	19,547	0,476	0,474	0,480	4,219	0,514	0,519	0,499	11,883	0,513	0,516	0,507	19,547	0,490	0,500	0,49931386
156	2864,73	Pasłęk	TFr	5,500	0,531	0,521	0,508	15,099	0,500	0,478	0,490	24,698	0,460	0,467	0,466	5,500	0,544	0,572	0,535	15,099	0,544	0,530	0,526	24,698	0,548	0,555	0,541002721
157	2864,73	Pasłęk	TFr	5,500	0,510	0,507	0,507	15,099	0,462	0,454	0,455	24,698	0,435	0,427	0,429	5,500	0,487	0,506	0,490	15,099	0,438	0,452	0,448	24,698	0,417	0,411	0,413913719
158	2886,82	Pasłęk	BFr	3,203	0,585	0,575	0,568	8,623	0,551	0,553	0,560	14,043	0,533	0,525	0,536	3,203	0,564	0,585	0,593	8,623	0,552	0,545	0,562	14,043	0,541	0,537	0,536472404
159	2830,05	Pasłęk	BFr	2,810	0,831	0,843	0,774	5,467	0,832	0,836	0,847	8,123	0,748	0,783	0,764	2,810	0,745	0,704	0,730	5,467	0,805	0,696	0,798	8,123	0,644	0,646	0,644538914
160	2831,17	Pasłęk	BFr	1,530	1,156	1,112	1,112	4,186	0,949	0,984	0,983	6,843	0,901	0,916	0,896	1,530	0,699	0,826	0,766	4,186	0,634	0,599	0,614	6,843	0,575	0,582	0,595108696
161	2832,24	Pasłęk	BFr	2,477	0,670	0,681	0,624	5,133	0,687	0,697	0,701	7,790	0,706	0,689	0,684	2,477	0,704	0,701	0,722	5,133	0,558	0,573	0,587	7,790	0,498	0,526	0,501449275
162	2834,17	Pasłęk	BFr	2,172	0,896	0,909	0,888	5,001	0,775	0,814	0,820	7,830	0,846	0,815	0,797	2,172	0,640	0,617	0,630	5,001	0,580	0,566	0,567	7,830	0,731	0,752	0,743858382
163	2834,39	Pasłęk	BFr	2,281	0,596	0,595	0,563	5,110	0,586	0,577	0,575	9,353	0,603	0,610	0,610	2,281	0,511	0,499	0,506	5,110	0,467	0,442	0,446	9,353	0,486	0,530	0,499470739
164	2838,07	Pasłęk	BFr	2,165	0,668	0,669	0,686	4,994	0,621	0,616	0,624	9,237	0,660	0,644	0,655	2,165	0,598	0,591	0,600	4,994	0,573	0,601	0,598	9,237	0,578	0,583	0,597458276
165	2854,64	Pasłęk	BFr	2,144	0,624	0,637	0,638	4,973	0,576	0,592	0,595	9,216	0,576	0,584	0,576	2,144	0,497	0,520	0,518	4,973	0,467	0,460	0,461	9,216	0,455	0,443	0,431246163
166	2872,21	Pasłęk	BFr	3,205	0,727	0,692	0,721	6,034	0,617	0,643	0,632	10,277	0,643	0,643	0,672	3,205	0,639	0,659	0,650	6,034	0,617	0,565	0,571	10,277	0,500	0,523	0,517753922
167	2873,72	Pasłęk	BFr	1,404	0,602	0,615	0,616	4,006	0,619	0,609	0,622	7,909	0,614	0,622	0,615	1,404	0,552	0,559	0,553	4,006	0,522	0,536	0,531	7,909	0,513	0,512	0,512255305
168	2868,18	Pasłęk	TFr	3,519	0,548	0,571	0,582	7,343	0,573	0,559	0,567	11,168	0,551	0,565	0,561	3,519	0,590	0,583	0,599	7,343	0,613	0,597	0,599	11,168	0,605	0,594	0,594349315
169	2869,07	Pasłęk	TFr	3,739	0,620	0,620	0,660	9,345	0,632	0,639	0,648	14,950	0,591	0,583	0,584	3,739	0,510	0,519	0,520	9,345	0,477	0,451	0,469	14,950	0,473	0,474	0,475815523
170	2779,70	Pasłęk	TFr	2,354	0,635	0,602	0,611	6,433	0,653	0,657	0,652	12,551	0,625	0,620	0,622	2,354	0,615	0,631	0,665	6,433	0,586	0,591	0,598	12,551	0,597	0,592	0,590022749
171	2775,81	Pasłęk	BFr	2,693	0,639	0,620	0,613	5,192	0,588	0,601	0,603	7,692	0,610	0,622	0,617	2,693	0,513	0,500	0,500	5,192	0,483	0,500	0,480	7,692	0,484	0,489	0,482047116
172	2776,22	Pasłęk	BFr	1,775	0,580	0,638	0,629	4,274	0,624	0,643	0,623	6,773	0,631	0,643	0,635	1,775	0,537	0,543	0,511	4,274	0,546	0,546	0,535	6,773	0,468	0,482	0,492066421
173	2776,45	Pasłęk	BFr	2,556	0,676	0,661	0,661	5,055	0,646	0,652	0,658	7,554	0,659	0,649	0,648	2,556	0,521	0,539	0,541	5,055	0,545	0,550	0,546	7,554	0,539	0,552	0,548056245
174	2777,36	Pasłęk	BFr	2,813	0,709	0,720	0,687	5,312	0,677	0,662	0,665	9,061	0,652	0,664	0,652	2,813	0,610	0,638	0,643	5,312	0,624	0,605	0,609	9,061	0,573	0,565	0,578540891
175	2785,41	Pasłęk	BFr	2,413	0,882	0,893	0,896	4,912	0,785	0,784	0,775	7,412	0,781	0,764	0,786	2,413	0,680	0,689	0,715	4,912	0,614	0,641	0,632	7,412	0,635	0,630	0,615747766
176	2826,25	Pasłęk	BFr	1,481	0,836	0,825	0,835	3,980	0,686	0,675	0,680	6,480	0,625	0,649	0,650	1,481	0,571	0,600	0,624	3,980	0,511	0,511	0,539	6,480	0,519	0,516	0,523625844
177	2807,15	Pasłęk	Tf	2,480	0,371	0,384	0,376	4,794	0,396	0,413	0,403	7,108	0,370	0,388	0,365	2,480	0,299	0,291	0,297	4,794	0,325	0,310	0,317	7,108	0,251	0,261	0,258463542
178	3920,92	Pasłęk	BFr	2,683	0,668	0,673	0,692	5,832	0,658	0,639	0,659	10,556	0,603	0,608	0,623	2,683	0,718	0,727	0,677	5,832	0,559	0,563	0,597	10,556	0,540	0,520	0,546986874
179	3921,63	Pasłęk	BFr	3,012	0,674	0,693	0,705	6,162	0,689	0,666	0,682	10,885	0,705	0,676	0,707	3,012	0,617	0,624	0,590	6,162	0,587	0,595	0,570	10,885	0,564	0,581	0,552003472
180	3927,37	Pasłęk	BFr	2,312	0,839	0,802	0,790	5,461	0,801	0,772	0,800	10,185	0,736	0,749	0,754	2,312	0,922	0,949	0,943	5,461	0,866	0,834	0,867	10,185	0,704	0,679	0,674706246
181	3929,09	Pasłęk	BFr	2,535	0,768	0,765	0,803	5,684	0,755	0,731	0,758	10,408	0,712	0,712	0,729	2,535	0,621	0,678	0,701	5,684	0,559	0,575	0,594	10,408	0,601	0,580	0,604689864
182	3936,17	Pasłęk	BFr	1,725	0,529	0,527	0,520	4,995	0,451	0,421	0,449	N/A	N/A	N/A	N/A	1,725	0,389	0,359	0,406	4,995	0,288	0,310	0,323	N/A	N/A	N/A	N/A
183	3935,63	Pasłęk	BFr	3,138	0,596	0,534	0,578	7,469	0,534	0,548	0,555	N/A	N/A	N/A	N/A	3,138	0,469	0,419	0,450	7,469	0,397	0,363	0,387	N/A	N/A	N/A	N/A